Review of Rarefied Gas Effects in Hypersonic Applications

Eswar Josyula and Jonathan Burt
U.S. Air Force Research Laboratory
Wright-Patterson Air Force Base, Ohio, USA

eswar.josyula@wpafb.af.mil, jonathan.m.burt@nasa.gov

ABSTRACT

Rarefied gas phenomena are found in a wide variety of hypersonic flow applications, and accurate characterization of such phenomena is often desired for engineering design and analysis. In atmospheric flows involving high Mach numbers and/or low densities, underlying assumptions in a continuum fluid dynamics description tend to break down, and distributions of both molecule velocity and internal energy modes can depart significantly from equilibrium. In this paper, characteristics of rarefied and nonequilibrium gas flows are discussed, and several numerical methods for rarefied flow simulation are outlined. A variety of hypersonic flow applications are presented, and additional discussion is provided for directions of current and future research.

1.0 INTRODUCTION

The field of rarefied gas dynamics is concerned with gas flow problems that do not conform to a continuum description; in particular, flows for which the Knudsen number – defined as the ratio of the mean free path to some characteristic length – is greater than that required to approximate the flow as a continuous medium. The mean free path is in turn defined as the average distance, typically in a reference frame which moves with the flow, that a molecule travels before colliding with another molecule. Traditional continuum gas dynamics models tend to break down due to gradient transport assumptions for diffusion terms in continuum equations of mass, momentum, and energy conservation. More generally, in a rarefied flow, the effect of intermolecular collisions to drive the distribution of molecular velocities toward the equilibrium limit (called a Maxwellian velocity distribution) is insufficient to maintain a near-equilibrium distribution. As a result, equilibrium assumptions underlying the continuum Navier-Stokes gas dynamics conservation equations become invalid, and detailed characterization of the velocity distribution function is required for accurate numerical simulation of the flow.

The above characteristics are typically found where length scales of gradients for the macroscopic quantities are on the order of the molecular mean free path of the gas. If the Knudsen number is used to characterize the degree of rarefaction effects, then we can expect rarefied flow to result from either a large mean free path or small characteristic length scales. Gas flow problems involving large mean free paths are often encountered in high altitude atmospheric flows, such as those around reentry vehicles and spacecraft in low Earth orbit; vacuum systems as used in industrial processes including chemical vapor deposition and freeze drying; and in low density plume flows from spacecraft or rockets. Flow problems for which rarefaction effects occur due to small length scales include hypersonic atmospheric flows, where local characteristic flow lengths may be very small inside thin shock and boundary layer regions; low speed flows through or around micro-electro-mechanical systems (MEMS); and other mechanical devices – such as computer hard drives – which involve small air gaps.

Early applications of rarefied gas dynamics involved problems in vacuum technology, but the field has had a major impact on aerothermal analysis and design of spacecrafts, satellites, missiles, etc. flying at high altitudes [1, 2]. In these applications, rarefaction effects become important due to very low densities and/or very high Mach numbers. In recent years, however, several applications have emerged for which

Report Documentation Page

Form Approved
OMB No. 0704-0188

1. REPORT DATE	2. REPORT TYPE	3. DATES COVERED
JAN 2011	**N/A**	**-**

4. TITLE AND SUBTITLE	5a. CONTRACT NUMBER
Review of Rarefied Gas Effects in Hypersonic Applications	5b. GRANT NUMBER
	5c. PROGRAM ELEMENT NUMBER
6. AUTHOR(S)	5d. PROJECT NUMBER
	5e. TASK NUMBER
	5f. WORK UNIT NUMBER
7. PERFORMING ORGANIZATION NAME(S) AND ADDRESS(ES) **U.S. Air Force Research Laboratory Wright-Patterson Air Force Base, Ohio, USA**	8. PERFORMING ORGANIZATION REPORT NUMBER
9. SPONSORING/MONITORING AGENCY NAME(S) AND ADDRESS(ES)	10. SPONSOR/MONITOR'S ACRONYM(S)
	11. SPONSOR/MONITOR'S REPORT NUMBER(S)

12. DISTRIBUTION/AVAILABILITY STATEMENT
Approved for public release, distribution unlimited

13. SUPPLEMENTARY NOTES
See also ADA579248. Models and Computational Methods for Rarefied Flows (Modeles et methodes de calcul des coulements de gaz rarefies). RTO-EN-AVT-194

14. ABSTRACT
Rarefied gas phenomena are found in a wide variety of hypersonic flow applications, and accurate characterization of such phenomena is often desired for engineering design and analysis. In atmospheric flows involving high Mach numbers and/or low densities, underlying assumptions in a continuum fluid dynamics description tend to break down, and distributions of both molecule velocity and internal energy modes can depart significantly from equilibrium. In this paper, characteristics of rarefied and nonequilibrium gas flows are discussed, and several numerical methods for rarefied flow simulation are outlined. A variety of hypersonic flow applications are presented, and additional discussion is provided for directions of current and future research.

15. SUBJECT TERMS

16. SECURITY CLASSIFICATION OF:			17. LIMITATION OF ABSTRACT	18. NUMBER OF PAGES	19a. NAME OF RESPONSIBLE PERSON
a. REPORT **unclassified**	b. ABSTRACT **unclassified**	c. THIS PAGE **unclassified**	**SAR**	**40**	

strong rarefaction effects occur as a result of small length scales associated with the flowfield geometry; one example of this is the MEMS device. In this paper, however, we will be primarily concerned with the applications of rarefied gases in hypersonic flows.

2.0 RAREFIED FLOW PHENOMENA

2.1 Mean Free Path and Various Flow Regimes

Rarefied gas flows are primarily classified in three flow regimes:

- $0.01 < Kn < 0.1$ Slip flow regime
- $0.1 < Kn < 10$ Transitional regime
- $Kn > 10$ Free molecular regime

Applications in slip flow regime manifest mainly near the boundaries of vehicles in high speed flight, as the so called velocity slip and temperature jump phenomena, which are treated by special boundary conditions. For the rest of the flowfield, the continuum gas dynamics equations are still valid. For the other extreme of the free molecular regime where *Kn* is high, the gas is very rarefied. In this regime, where the mean free path is much larger than the characteristic dimension of the body, the collisions occur infrequently even after the particles hitting the surface reflect away. In the transitional regime ($0.1 < Kn < 10$), both the collisions between particles and with the surface assume importance, hence this is an area of rarefied gas dynamics with considerable body of research. The primary thrust of this paper is for flows in the transitional regime.

In the molecular description of a gas, the kinetic theory is based on the hypothesis that the gas is composed of molecules. Although for a gas at rest, the molecules are separated by distances large enough that they interact weakly with each other. But when the molecules interact strongly they are considered to be collisions. In the treatment of interactions, if the time average of potential energy can be neglected compared with the kinetic energy, the gas is called perfect. When this condition is not satisfied, the gas is called van der Waals gas. The vast body of the literature on rarefied gas dynamics deals with gases that are perfect. In practice, gases of neutral molecules up to pressures of hundreds of atmospheres are considered perfect. Another useful way to classify the regime is with pressure. For gases even up to very high pressures, three-body collisions are small in comparison with two-body collisions, and here, Classical Newtonian mechanics is used to describe the motion of the molecules except where quantum effects become important. In addition to the importance of quantum effects at very low temperatures and for light molecules, which we will not consider, quantum effects must be taken into account in aerospace applications for inelastic collisions of atoms and molecules where the internal degrees of freedom are excited. The potential of these molecular interactions may be calculated only be the use of quantum mechanics.

2.2 Breakdown of Navier-Stokes Equations

The Navier Stokes equation are derived assuming only small deviations from equilibrium as characterized by a Maxwellian distribution function. In the equilibrium state of a gas, the distribution of molecular energy states does not vary with time. Although intermolecular collisions occur, and energy is exchanged in collisions, the gas maintains the same number of particles in a given energy state. Similarly, if the gas were to undergo a reaction, the equilibrium state would imply that the rate at which the forward reaction progresses is exactly equal to the rate at which the reverse reaction progresses, such that the composition of the gas does not vary over time. On the other hand, a state of nonequilibrium is often a transient state; it

is the process by which the gas approaches a new equilibrium state.

The continuum equations are also invalid in regions of very low density. When a relatively small number of particles occupy the flowfield of interest, the continuum hypothesis is obviously invalidated as large regions of the flowfield may contain no particles at all. This may occur naturally as in the upper atmosphere, or may be caused by rapid expansion of the flow. In this case, the collision rate drops drastically and the continual decrease in temperature predicted by the continuum equations cannot be maintained. This is because as the number of collisions experienced by the particlescontinues to decrease, the translational temperature eventually levels out or “freezes" as the free molecular regime is approached [3, 4, 5]. Alternatively, when the length scale of consideration is on the order of the mean free path in the gas, the flow may “appear" rarefied even at normal densities, and the continuum hypothesis will no longer hold. This case is of practical interest for the analysis of microscale aerodynamics and fluid flow through micro-electro-mechanical systems (MEMS) [6].

The validity of the continuum equations is inherently tied to the collision rate in the gas. Letting ν represent the intermolecular collision rate and t_f represent the characteristic flow time, the Knudsen number Kn may be defined as follows.

$$Kn = \frac{1}{\nu t_f} \tag{1}$$

Alternatively, letting $\bar{c}$ be the mean molecular speed, λ the mean free path (the average distance traveled by a molecule before encountering a collision), and L represent a characteristic length scale, the above equation becomes

$$Kn = \frac{1}{\nu t_f} = \frac{1}{(\bar{c}/\lambda)(L/\bar{c})} = \frac{\lambda}{L} \tag{2}$$

The validity criterion for the continuum equations has been stated as $Kn << 1$. However, the choice of characteristic length scale may be somewhat ambiguous. Choosing a length scale based upon the geometry over which the flow is considered results in a parameter which may describe globally how well the continuum equations apply, however, it does not address the properties of the local flow physics which may occur. A better choice is to consider a local length scale related to the physics occurring in the flowfield. This may be a quantity such as a shock thickness, boundary layer thickness, or some other length associated with the local flow physics.

The limits shown in Figure 1 are based upon experimental observations and should not be thought of as hard limits or having a rigorous mathematical basis. Indeed this is the very reason it is desired to study the criteria for continuum breakdown. The Euler equations are strictly based upon the Maxwellian velocity distribution, which is the prevailing distribution when the gas is in equilibrium. Furthermore, as they include no viscous terms, they are only valid at very low Knudsen number, or when the collision rate becomes quite large. When this occurs, the gas is able to redistribute its energy to accommodate varying conditions almost instantly, and the flow is practically in equilibrium everywhere.

The Navier-Stokes equations exhibit an extended Knudsen number validity over the Euler equations as seen in Figure 1. Pinpointing exactly where they become invalid is somewhat difficult to predict, but it is generally accepted that this occurs at Knudsen numbers somewhere around 0.1 [4]. The Navier-Stokes equations can be derived by using the first Chapman-Enskog correction to the Maxwellian distribution function [7] [8]. This means that the Navier-Stokes equations are based upon a small departure from the equilibrium distribution function and will fail in regions of significant nonequilibrium.

Many flow scenarios contain several physical processes that exhibit local Knudsen numbers at many different locations on this spectrum. This is particularly the case in some hypersonic flows. Consider a typical blunt body in hypersonic flow. The physics involved with the associated structure of the strong shocks invalidate the continuum equations. Aft of the shock the continuum equations may hold. Close to the body, strong gradients exist across the boundary layer and the process of activating the internal modes of the gas may occur in nonequilibrium fashion. Further downstream the flow may expand around the body to the point at which the density is too low for the continuum equations to hold. Such a mixed flowfield exemplifies why a hybrid method may be desirable, illustrates the importance of understanding where the continuum equations are and are not valid, and emphasizes the need for a good understanding of nonequilibrium phenomena.

In the past, several parameters have been examined in an attempt to quantify continuum breakdown. For obvious reasons, many of the initial investigations considered parameters in the form of a Knudsen number based upon the local flow physics. This approach is based on the observation that if flow variables change over relatively small distances in comparison to the local mean free path, it is unlikely that enough collisions are experienced for the gas to reach equilibrium at the new conditions. Bird [3] was one of the first to examine the validity of such a parameter using DSMC. He did so in the context of nonequilibrium resulting from expansions of the gas. In doing so, he suggested the following parameter as a means of quantifying equilibrium breakdown.

$$P = \frac{1}{v}\left|\frac{D(\ln\rho)}{Dt}\right| \tag{3}$$

where ρ is the density of the gas. In the case of one dimensional steady flow, this becomes

$$P = \frac{u}{\rho v}\left|\frac{d\rho}{dx}\right| = M\sqrt{\frac{\pi\gamma}{8}}\frac{\lambda}{\rho}\left|\frac{d\rho}{dx}\right| \tag{4}$$

where u is the bulk gas velocity and M is the Mach number in the gas. Bird found that a value of P greater than 0.02 tended to predict the onset of nonequilibrium well.

While this parameter seems to indicate continuum breakdown well in the specific case of gaseous expansions, it does not predict nonequilibrium well in regions of low velocity. As seen in the above equation, the Mach number dependence will drive P to zero in regions of low velocity no matter what the degree of nonequilibrium. Boyd proposed examining a Knudsen number based upon the gradient local length (GLL) as a means of examining continuum breakdown [9].

$$Kn_{GLL} = \frac{\lambda}{Q}\left|\nabla Q\right| \tag{5}$$

where Q is some flow property of interest. The dependence of Bird's parameter on a gradient based local Knudsen number is readily seen in the following equation.

$$P = M\sqrt{\frac{\pi\gamma}{8}}Kn_{\rho} \tag{6}$$

where $Kn_{\rho} = \frac{\lambda}{\rho}\left|\frac{d\rho}{dx}\right|$ is the Knudsen number based upon the gradient local length of the density. Determining which flow variable is the best to use for examining continuum breakdown is nontrivial, and

may vary from one flow scenario to another. For this reason, Wang and Boyd [10] proposed using the following criterion

$$Kn_{\max} = \max\left\{Kn_{\rho}, Kn_{T}, Kn_{V}\right\} \tag{7}$$

where Kn_T is the Knudsen number based upon the gradient local length of the temperature, and Kn_V is the Knudsen number based upon the gradient local length of the fluid velocity. They proposed that significant nonequilibrium was indicated when this parameter became greater than about 0.05

Unfortunately, while such parameters are relatively easy to compute, they do not necessarily have a firm theoretical grounding. Qualitatively, they make some sense, in that many forms of nonequilibrium are set into motion by the presence of strong gradients in the flow variables. Such parameters are also tied to the traditional understanding of a Knudsen number restriction on the continuum equations. However, the fact that multiple parameters must be computed suggests that the continuum prediction criterion is problem dependent at this stage of development. It should be noted that the computation of the heat flux and shear stress terms involves the combination of a number of flow gradients. This partially speaks to why multiple gradient-based Knudsen parameters are required to obtain a reasonable predictive capability.

2.3 Nonequilibrium Internal Energy Excitation

Thermal nonequilibrium among the internal modes of motion of the molecular species in supersonic and hypersonic flows has major influences on flowfield temperatures, radiation signatures, and aerodynamic heating. Prediction of such flowfields by computer modeling techniques requires a detailed knowledge of the rates and mechanism of energy storage and transfer among the internal modes of molecular motion. Among the large body of literature, we mention a few: Anderson [11], Capitelli [12], Chernyi et al.[13], Rich et al. [14], and Adamovich et al. [15].

The various modes of motion for diatomic gas molecules which are of interest in aerothermodynamics are translation, rotation, vibration, electronic and the mutual interaction of these modes. In addition, molecules can dissociate and ionize. For our purposes of engineering interest, translational motion can be described by classical mechanics and is treated in other sections in this paper. However, to quantify the degree of nonequilibrium in the internal energy modes one would have to consider the internal energy modes of rotation, vibration, and electronic excitation, all of which are quantized. When the gas is in a state of thermal equilibrium, the distribution of internal energy among the various modes is said to be governed by a Maxwell-Boltzmann distribution, which can be written as the fractional number of molecules n_i in the ith internal energy state as:

$$\frac{n_i}{N} = \frac{g_i}{Q_{\text{int}}} \exp\left(-\frac{E_{i,\text{int}}}{kT}\right) \tag{8}$$

where the internal partition function Q_{int} is given by

$$Q_{\text{int}} = \sum_i g_i \exp\left(-\frac{E_{i,\text{int}}}{kT}\right) \tag{9}$$

where $N = \sum_i n_i$ is the total number of atoms and molecules and g_i is the statistical weight of the ith internal energy state, k is the Boltzmann constant, and T is the kinetic temperature of the gas. In this section, we will review some recent advances concerning situations where the rate of relaxation to the equilibrium distribution given by Eq. (8) is slow relative to the mean collision time. Each of the energy

modes must undergo a finite number of molecular collisions, governed by a relaxation time, in order to equilibrate with the translational mode. The relative magnitude of the relaxation times may be stated as follows:

$$\tau_0 \approx \tau_T < \tau_R << \tau_V < \tau_d$$

where τ_0 is the mean collision time and τ_T, τ_R, τ_V, and τ_d are respectively the relaxation times for translational, rotational, vibrational energy modes and dissociation.

For a diatomic molecule N_2, the symbolic equations governing the Vibrational-Translational (VT) transitions responsible for the variation of the particles distributed in the ith vibrational level are

$$N_2(i) + N_2 \rightleftharpoons N_2(i') + N_2 \tag{10}$$

and the equations governing the Vibration-Vibration (VV) process are

$$N_2(i) + N_2(j) \rightleftharpoons N_2(i') + N_2(j') \tag{11}$$

The equations governing the dissociation process, considering dissociation to take place from any vibrational level, are

$$N_2(i) + M \rightleftharpoons 2N + M \tag{12}$$

The kinetics of vibrational energy exchanges among the quantum states are simulated using the vibrational master equations [16], for which the population distributions are calculated with

$$\dot{\omega}_V = \frac{1}{\mathcal{M}} \begin{pmatrix} \sum_{i'} \left[k_{VT}(i' \to i)\rho_{v'}\rho - k_{VT}(i \to i')\rho_{v'}\rho \right] \\ + \sum_{j,i,j'} \left[r_{VV}(i', j' \to i, j)\rho_{i'}\rho_{j'} - r_{VV}(i, j \to i', j')\rho_i\rho_j \right] \\ + \left[-k_{VD}(i \to \text{continuum})\rho_i\rho_{N_2} - \bar{k}_{VD}(\text{continuum} \to i)\rho_N\rho_N \right] \end{pmatrix} \tag{13}$$

where $\mathcal{M}$ is the molecular weight and ρ indicates the relative population at a given state. Energy exchanges consist of multiquantum transitions for VT and VV processes. Additionally dissociation can occur from any of the vibrational states to continuum. The VT process is associated with the rate coefficient k_{VT} where the molecule loses or gains a number of vibrational quanta. The de-excitation rate from i' to i for colliding molecules is denoted by $k_{VT}(i' \to i)$, the inverse collision from i to i' by $k_{VT}(i \to i')$. When considering VV exchanges, the initial and final vibrational states of each collision partner must be identified; thus the transition rate from i' to i and j' to j is given by $r_{VV}(i',j' \to i,j)$. Consistency of the rate coefficient with the principle of detailed balance is enforced.

The vibrational energy of the diatomic molecules N_2, treated as anharmonic oscillators, is given in terms of the quantum level energies and state densities by

$$e_{vib} = \sum_{i=0}^{i^*} \frac{\rho_i}{\rho} \varepsilon_i \tag{14}$$

In this equation, ρ_i/ρ is the fractional population in the ith vibrational level and ε_i is the quantum level

energy given by the third-order approximating formula

$$\frac{\varepsilon_i}{hc} = \omega_e\left(i-\frac{1}{2}\right) - \omega_e x_e\left(i-\frac{1}{2}\right)^2 + \omega_e y_e\left(i-\frac{1}{2}\right)^3 \qquad i = 1,2,... \tag{15}$$

where h is the Planck's constant and c is the speed of light. Here, ε_1 denotes ground state vibrational energy, ε_2 denotes first excited state, and so on. For nitrogen, the spectroscopic constants are given by ω_e = 2358.57 cm^{-1}, $\omega_e x_e$ = 14.324 cm^{-1}, and $\omega_e y_e$ = -0.00226 cm^{-1}. When i^* = 48, the vibrational energy value exceeds the dissociation energy of 9.86 eV.

Vibrational relaxation involves two widely different time scales, associated with the VT and VV processes. The relaxation in diatomic gases may be significantly affected by the rapid VV transfer processes. In VV exchange collisions between two molecules, the vibrational quanta in one molecule increases while in the other it decreases. Due to anharmonicity, this results in a net energy transfer with the translational mode. Such transfers occur with high probability because the net change in energy of each VV transitions is small relative to VT transitions. In fact, the difference in time scales is often $\tau_{VV} << \tau_{VT}$ so that we can identify the VV rates as "fast" rates and the VT rates as the "slow" rates in a relaxation process. During the initial stages of relaxation, the VV exchanges dominate and during the remaining bulk of relaxation, the VT transitions are also effective. In a single component system of anharmonic oscillators, VV processes may have significant effects for all quantum levels except the upper levels. For large vibrational quantum numbers and closely spaced energy levels of an anharmonic oscillator, the VT transitions are rapid. The population distribution of these upper levels is normally well described by a vibrational temperature equal to the translational temperature.

For VT processes which transfer energy between the vibrational and translational degrees of freedom, the energy exchange is of the order of the vibrational energy spacing. VV processes, affected by the anharmonicity of the system, influence the flow of vibrational energy transfer between lower and upper levels. We define T_{vib} as the vibrational temperature based on relative populations at all vibrational levels, and T_{fl} is the temperature based on the ratio between first excited state and ground state populations. For $T_{fl} \neq T_{vib}$ the vibrational distribution differs from that of a Boltzmann, the deviation increasing with increasing vibrational quantum level. For $T_{fl} < T_{vib}$ anharmonicity causes the underpopulation of upper vibrational levels, whereas for $T_{fl} > T_{vib}$ it causes an overpopulation. The steady-state nonequilibrium vibrational distribution function in a one component system of anharmonic oscillators was derived by Treanor, Rich and Rehm [17]. Owing to the high vibration-vibration energy exchange in the anharmonic oscillators, the low to intermediate vibrational levels achieved a concave-upward population distribution known as the Treanor distribution. A popular assumption in modern computations of hypersonic aerodynamic simulations is to treat the molecule as a simple harmonic oscillator where the vibrational energy is modeled by the Landau-Teller method [8].

The rates (cm^3/s) for VV and VT exchange in nitrogen are presented in Figure 2 at 6000K. The VT rate corresponds to $j+1 \rightarrow j$ increases monotonically with the quantum level vibrational energy. Two relevant VV exchanges are also presented, both weighted by the relative equilibrium population of the vibrational state of the collision partner: The rate of weighted VV exchange involving the ground state increases with quantum level vibrational energy and then decreases due to increasing disparity of the energy being exchanged. The rate of population-weighted resonant exchange increases with vibrational quantum number initially and then decreases due to the reduced population associated with the excited state of the collision partner.

Also shown in Figure 2 is the equilibrium dissociation rate. This is the value required to support the equilibrium dissociation rate from a single, given vibrational state. In the ``ladder model" the state of interest is the last bound vibrational state. For a given set of VV and VT transition rates, the relative

importance of the VV terms $r_{j+1,j}^{n,n+1}$, the VT term $k_{j+1,j}$, and the dissociation term can be assessed. It can be concluded that for nitrogen at these temperatures, the dissociation probability for the last state is high relative to both the weighted VV and VT rates, and that VT is more important than VV. Regarding depletion of the dissociating state, one would anticipate that depletion will be significant for Rate Set 1 (Figure 1a) [18, 19] because the dissociation rate exceeds the V-T rate considerably and not quite as significant for Rate Set 2 (Figure 1b) [20]. Since the VT probabilities are higher than those of weighted VV energy transfers, the effect of VV on the population depletion is negligible, as shown in Figure 2 [16]. The aforementioned case is a good example of the need to have reliable transition rates for accurate predictions with state specific models.

Figure 3 illustrates VT multiquantum and single-quantum rate coefficients from the 25th vibrational quantum level (i = 25) to lower levels (i' = 15, 23, 24) [21, 22, 23]. The multiquantum rate coefficients (i' = 15, 23) become comparable to that of single quantum (i' = 24) with increasing translational temperature. It may be concluded that multiquantum processes are important at high temperature conditions. On the contrary, large multiquantum transitions are less probable at lower temperatures (see i' = 15 curve) since collision energies are not high enough to permit large energy jumps. Because the energy levels are closer to each other with increasing vibrational quantum numbers, the vibrational jumps are more probable at moderate and high vibrational levels. Therefore, one may expect from Figure 3 that the lower vibrational levels are populated mainly by single-quantum transitions.

Figure 4 shows the influence of multiquantum VT processes on the evolution of the translational temperature behind the standing shock wave. The translational temperature due to single-quantum transitions decays much more gradually with distance. One can see that at the higher temperatures, immediately behind the shock front, the effect of multiquantum transitions is very high, leading to a faster rate of equilibration. The differences in macroscopic quantities from single- and multiquantum effects can be attributed to the difference in the total transition probability of a VT exchange; i.e. for the probability to sum up to unity, all multiquantum transitions have to occur. This constraint would imply that the assumption of single quantum energy exchanges will result in a total probability less than unity. The difference in the total probability of energy exchange causes the mean energy transfer to be different for the single and multiquantum transitions, as seen for the translational temperature difference in Figure 4.

Figure 5 illustrates the vibrational population distribution as a function of the vibrational energy in the quantum energy states, for multiquantum and single-quantum processes at various distances (0.01 and 0.03 cm) behind the shock. It is clear that multiquantum mechanisms populate intermediate and high levels more quickly, i.e. for i > 10, vibrational energy greater than 3 eV. For the multiquantum transition case, the upper vibrational levels follow a Boltzmann distribution at the higher temperature. However, concentrations of the low energy levels (i < 10, vibrational energy less than 3 eV) vary and decrease slowly during the relaxation of the gas flow behind the shock wave. The slow variation occurs because VT transitions in the lower vibrational states are required to overcome a large energy gap, and consequently single quantum and multiquantum collisions are less effective. The concentrations of the lower vibrational levels experience a lag because molecules jump to higher energy states due to VT exchanges. The inset in Figure 5 shows that the population is smallest in the low-lying states when the flow reaches equilibrium downstream of the shock wave. In the vicinity of the shock wave, at the locations of 0.03 cm and 0.01 cm, the population in these low-lying states is higher when multiquantum jumps are considered and highest with single quantum jumps. However, with an increase in vibrational levels, the equilibrium population increases to a higher value than the nonequilibrium population (note the crossing of equilibrium and nonequilibrium curves).

3.0 MODELING RAREFIED GAS FLOWS

3.1 Direct Boltzmann Equation Solution Methodology

For a continuum description of a gas flow, we specify the velocity field, stress tensor, and heat flux vector and additionally, the three thermodynamic variables of density, pressure, and temperature. The stress tensor and heat flux vector are not usually treated as independent variables, such that a minimal fluid mechanical description requires five independent variables. The statistical mechanical description of the same system requires 6*N* variables, where *N* is the number of molecules in the system; typical values for *N* are about 1023. These variables are usually taken to be 3*N* spatial coordinates, and 3*N* conjugate momenta of the constituent molecules. As one can see, the large number of degrees of freedom in the microscopic description distinguishes it from the macroscopic description.

The Boltzmann Equation is the governing equation in the microscopic description of a dilute gas flow, and is a nonlinear integro-differential equation for a probability distribution function which describes statistically the state of the particles as a function of time. The equation is limited in its applicability to systems for which the following conditions are met:

- The density is sufficiently low so that only binary collisions between the constituent molecules need to be considered.
- The spatial dependence of gas properties is sufficiently low so that collisions can be thought of as being localized in the physical space.
- The intermolecular potential is of sufficiently short range.

The Boltzmann equation may be written as

$$\frac{\partial f}{\partial t} + \boldsymbol{\xi}\frac{\partial f}{\partial \boldsymbol{x}} = I(f) \tag{16}$$

where

$$I(f) = \int_{\mathcal{R}^3}\int_{\mathcal{R}^2}\left(f(\boldsymbol{x},\boldsymbol{\xi}',t)\,f(\boldsymbol{x},\boldsymbol{\xi}_1',t) - f(\boldsymbol{x},\boldsymbol{\xi},t)\,f(\boldsymbol{x},\boldsymbol{\xi}_1,t)\right)B\,d\sigma\,d\boldsymbol{\xi}_1 \tag{17}$$

The right side of Eq. (17) is a nonlinear phase space integral which describes the effect of intermolecular collisions; integration is performed over all velocity space and over the surface of a sphere of influence. The collision term $I(f)$ is a function of the differential collision cross-section (related to B), pre-collision velocities ($\boldsymbol{\xi}$, $\boldsymbol{\xi}_1$) and post-collision velocities ($\boldsymbol{\xi}'$, $\boldsymbol{\xi}_1'$). In this representation, we assume both molecular chaos and binary collisions [24]. A detailed explanation of the Boltzmann collision term $I(f)$ is beyond the scope of the current discussion, but thorough descriptions of this term are provided by Vincenti and Kruger [8], Cercignani [24] and Bird [4]. The term f, known as the distribution function, describes the many-body system and can be integrated in velocity space to determine macroscopic flow quantities. More specifically, $f(\boldsymbol{x},\boldsymbol{\xi},t)$ is the fraction of all particles in the spatial volume element around $\boldsymbol{x}$ which have their velocity vectors between $\boldsymbol{\xi}$ and $\boldsymbol{\xi}75^3\boldsymbol{\xi}$. In other words, f is the conditional probability of finding a particle in the velocity space volume element $d^3\boldsymbol{\xi}$ around $\boldsymbol{\xi}$, provided that the particle is located in the configuration space volume element $d^3\boldsymbol{x}$ around $\boldsymbol{x}$. Integrating f over its velocity argument will then give an expression for the expected gas number density n in the volume element $d^3\boldsymbol{x}$ about $\boldsymbol{x}$.

$$n(\boldsymbol{x},t) = \int_{\mathcal{R}^3} f(\boldsymbol{x},\boldsymbol{\xi},t)\,d^3\boldsymbol{\xi} \tag{18}$$

More generally, any macroscopic flow quantity $\bar{Q}$ averaged over velocity space may be calculated as

$$\bar{Q}(\boldsymbol{x},t)=\frac{1}{n(\boldsymbol{x},t)}\int_{\mathcal{R}^3} f(\boldsymbol{x},\boldsymbol{\xi},t)Q(\boldsymbol{\xi})d^3\boldsymbol{\xi} \tag{19}$$

where Q is a function of $\boldsymbol{\xi}$, and integrals in both Eqs. (18) and (19) are performed over all velocity space. For example, the gas bulk velocity is found by setting $Q = \boldsymbol{\xi}$.

In a direct numerical solution of the Boltzmann equation, Eq. (16) is solved on a grid with cell size $\Delta\boldsymbol{x}$ in physical space and on a velocity grid with cell size $\Delta\boldsymbol{\xi}$ introduced in a finite volume domain. On the basis of three-dimensional delta functions, the distribution function and the collision integral can be represented in a discretized form [25]. After determining the expansion coefficients for the collision integral, the problem is reduced to solving the system of equations

$$\frac{1}{\Delta t}\left(f_\gamma^{t+\Delta t}-f_\gamma^{t}\right)+\boldsymbol{\xi}_\gamma\frac{\Delta_x f_\gamma^t}{\Delta\boldsymbol{x}}=I_\gamma \tag{20}$$

by the finite difference method. Here γ is a phase space index, I_γ is a discretized approximation of the collision integral, Δt is the time step interval, t is the elapsed simulation time, and Δ_x indicates a difference in f between neighboring nodes in physical space.

The distribution function normalized by their respective peak values at four x-locations are presented for a Mach 5 shock wave in Figure 6, as calculated using a discrete velocity Boltzmann technique. The spatial locations are: far upstream, slightly upstream of the center of the shock, slightly downstream of the center location, and far downstream. The asymptotic form of the distribution function at the upstream and downstream location is given by the shifted Maxwellian prescribed by the Rankine-Hugoniot conditions. One can see a non-Maxwellian distribution in $x/\lambda = 0$ and bimodal distribution at $x/\lambda = 0.8$. The probability distribution function of coarse and fine velocity grids is shown in Figure 7. The relative magnitudes of the peaks are significantly different in the shock wave (Figure 7a and b) and close to each other far downstream (Figure 7c).

For hypersonics applications, direct numerical solution methods for the discretized Boltzmann equation have historically received less attention than other rarefied flow simulation methods, such as direct simulation Monte Carlo (DSMC) [4]. This can be attributed in part to the often prohibitive computational expense and memory requirements in solving the discretized Boltzmann equation on a sufficiently refined velocity grid. In a recent study involving two dimensional simulation of a Mach 4 monatomic gas flow over a cylinder, a direct Boltzmann calculation required roughly 500 times more CPU time than a DSMC simulation [26]. Direct Boltzmann methods do, however, have attributes which may make them preferred techniques under certain conditions. In particular, these methods do not suffer from the statistical scatter problems inherent in DSMC, which can make these methods better suited to simulation of rarefied subsonic flows and to integration with continuum flow solvers in a strongly coupled hybrid scheme. One such hybrid scheme is implemented in the Unified Flow Solver (UFS) code [27]; this code has recently been applied to a number of hypersonics problems involving mixed rarefied and continuum flow regimes, and has shown considerable promise as an engineering analysis tool [28, 29].

Several current research topics for direct Boltzmann methods are focused on efficiency improvements. These topics include development of Boltzmann schemes with higher order accuracy in velocity space; velocity grid adaptation for local optimization of the velocity grid based on variation in Mach number and temperature; the use of low discrepancy sequences for efficient quasi-Monte Carlo evaluation of the Boltzmann collision integral; and preferential sampling of high probability velocity space nodes during collision integral evaluation.

3.2 Gas Kinetic Navier-Stokes Scheme

The Boltzmann equation expresses the behavior of many-particle kinetic system in terms of the evolution equation for the single particle gas distribution function. The simplified collision model given by the Bhatnagar Gross Krook (BGK) model [30] is formulated as

$$\frac{\partial f}{\partial t} + \boldsymbol{\xi} \frac{\partial f}{\partial \boldsymbol{x}} = \frac{1}{\tau}\left(f_{(0)} - f \right) \tag{21}$$

where $f_{(0)}$ is the equilibrium (i.e. Maxwellian) distribution function for which integration over all velocity space, as in Eq. (18), gives the local number density $n(\boldsymbol{x},t)$. The symbol τ in Eq. (21) represents a characteristic translational relaxation time, and is generally set to the reciprocal of the mean collision frequency at position $\boldsymbol{x}$ and time t. As described above, the distribution function f gives the number density per unit velocity space for molecules at position $\boldsymbol{x}$, velocity $\boldsymbol{\xi}$ and time t. The left hand side of Eq. (21) represents the free streaming of molecules in space, and the right side denotes the collision term. If the distribution function f is known, then macroscopic variables of the mass, momentum, energy and stress can be obtained by integration over the moments of molecular velocity. In the BGK model, the collision operator involves a simple relaxation to a local equilibrium distribution function $f_{(0)}$. The BGK model was proposed to describe the essential physics of molecular interactions, while neglecting details of the nonlinear collision integral in the full Boltzmann equation. Based on the above BGK model, the Navier-Stokes equations can be obtained with the Chapman-Enskog expansion (discussed in Section 3.3) truncated to the first order,

$$f = f_{(0)} + Kn\, f_{(1)} = f_{(0)} - \tau\left(\frac{f_{(0)}}{\partial t} + \boldsymbol{\xi} \frac{f_{(0)}}{\partial \boldsymbol{x}} \right) \tag{22}$$

where $f_{(0)}$ and $Kn\, f_{(1)}$ denote equilibrium and nonequilibrium components, respectively, of the distribution function f. With modifications to the characteristic collision time τ, the validity of the kinetic model is extended beyond that of the traditional Navier-Stokes equations [31, 32].

A kinetic Navier-Stokes method based on moments of the BGK equation, with its approximate collision terms, is very simple and attractive. Attributes include the mathematical simplicity of the collision term, and the lack of specific assumptions on intermolecular forces of the collision term. The BGK collision approximation is not considered rigorous theory, and one main disadvantage of the BGK method is that the relaxation time $\tau(\boldsymbol{x},t)$ must often be determined empirically for lack of a better way.

Figure 8 shows, for a Mach 3 shock wave, the profiles of density, temperature, viscous stress (xx-component) and streamwise component of heat flux. The agreement of the gas kinetic scheme results agree well with Ref. [33]. Figure 9 shows, for the Mach 5 shock wave, the density, mean temperature, and the streamwise and normal temperatures for the kinetic Navier-Stokes scheme and the Boltzmann solution. From a comparison of the density profiles in Figure 9a, one notes the excellent agreement of the density profiles for the Mach 5 shock wave. Note from Figure 9b and c that the starting location of elevated temperatures predicted by the kinetic Navier-Stokes scheme is more upstream than that of the Boltzmann solution.

3.3 Moment Methods

Another simplification to the Boltzmann equation is the well known Moment method described briefly in this paper from a historical perspective. Hilbert [34] discussed the existence and uniqueness of the Boltzmann equation, Eq. (16), by exploring a restricted class of solutions (which can be represented by a power series, involving a perturbation parameter), and showed that there exists a one-to-one mapping

between the distribution function f which is a solution of the Boltzmann equation and the first five moments of f as given by Eq. (19). These moments represent density, bulk velocity components and temperature. Hilbert's approach, although useful for obtaining Euler equations using the lowest order approximation, is impractical for obtaining the Navier-Stokes equations. In order to derive both Euler and Navier-Stokes equations from the Boltzmann equation, an approach developed independently by Chapman [35, 36] and Enskog [37] can be used. In the Chapman-Enskog approach, the distribution function f is expanded as a power series about the equilibrium distribution function $f_{(0)}$ as

$$f = f_{(0)} + \varepsilon f_{(1)} + \varepsilon^2 f_{(2)}^2 + \ldots \tag{23}$$

where ε can be directly related to the Knudsen number. In this approach, it is also assumed that time is not an explicit argument of the distribution function f and the time derivative of the first five macroscopic moments, but is an implicit argument by virtue of the dependence of f on the macroscopic moments and their spatial derivatives. This key assumption results in expansions that are quite different from those obtained from Hilbert's approach, especially in the splitting of the time derivative of f among various terms of the expansion.

A set of moment equations may be derived by substituting the right side of Eq. (23) for f, multiplying each term of Eq. (16) by powers of ξ, then integrating over all velocity space. It may be noted that in the near equilibrium limit (as ε tends to zero), the Maxwellian equilibrium distribution function $f_{(0)}$ is recovered, for which moment equations result in the Euler equations, wherein the viscous stress tensor and the heat flux vector are zero. Using a first order approximation of the Chapman-Enskog expansion of the Boltzmann equation, the Navier-Stokes equations can be recovered from the moment equations, where non-zero values of viscous stress tensor and heat flux vector (with dependence on the mean strain rate and temperature gradient respectively) are present. Second-order Chapman-Enskog expansions applied to the Boltzmann equation will result in moment equations called the Burnett equations, while higher order expansions result in the super-Burnett equations. The use of Burnett and super-Burnett equations can be challenging, as these equations are ill-posed and subject to numerical instabilities.

One of the models often used to approximate the Boltzmann collision term, Eq. (17), is the Bhatnagar-Gross-Krook model [30] mentioned in Section 3.2, which greatly simplifies the solution of the Boltzmann equation and the derivation of the evolution of macroscopic properties. Another interesting moment based approach was proposed by Grad [38], where the distribution function f is expanded in terms of a complete set of orthogonal polynomials (e.g. Hermite polynomials), whose coefficients correspond to velocity moments. This expansion is truncated by retaining terms up to a certain selected order, resulting in closed set of moment equations up to this order.

Although Grad's moment approach has been widely used for solution of the Boltzmann equation, it is best suited to problems for which the velocity distribution function can be expressed as a perturbation about the equilibrium (Maxwellian) distribution. In other words, Grad's method is not very efficient for treating problems with general non-equilibrium (non-Maxwellian) distributions, as Grad's moment method assumes that the zeroth order term of the expansion recovers the equilibrium distribution by virtue of the properties of Hermite polynomial (basis) functions.

In order to address such problems for treatment of non-equilibrium flows, it is plausible that an adaptive quadrature approach – where the form of the distribution function is not restricted to perturbations about an equilibrium distribution function – could offer certain advantages over conventional moment based approaches (e.g. Grad's moment approach). The implementation of such an approach also requires a detailed and efficient treatment of the collision operator. One such approach is the application of the direct quadrature method of moments (DQMOM) for solution of the full Boltzmann equation. In DQMOM, the velocity distribution function is approximated as a collection of discrete Dirac delta functions, with

associated weights and abscissas in phase space. In particular, the particle distribution function is given by a discrete sum of N Dirac delta functions, as

$$f\left(\boldsymbol{x},\boldsymbol{\xi},t\right)=\sum_{i=1}^{N} p_i\left(\boldsymbol{x},t\right)\delta\left(\boldsymbol{\xi}-\boldsymbol{\xi}_i\left(\boldsymbol{x},t\right)\right) \tag{24}$$

where $\delta(\boldsymbol{\xi}-\boldsymbol{\xi}_i) \equiv \delta(u-u_i)\delta(v-v_i)\delta(w-w_i)$, (u, v, w) are the components of $\boldsymbol{\xi}$, and the unknowns p_i and $\boldsymbol{\xi}_i$ denote the associated quadrature weights and abscissas in velocity space, respectively. Each quadrature node $i = 1 \ldots N$ has four unknowns: (pi, u_i, v_i, w_i) and hence there are $4N$ unknowns to be determined for each spatial location $\boldsymbol{x}$ at any point in time. The unknown weights and abscissas are obtained as solutions of their evolution equations (or moment equations in case of QMOM), which are in turn derived from the Boltzmann equation using constraints on generalized moments of velocity. These constraints on high order moments are derived based on the complex collision integral given as Eq. (17), without resorting to the use of simplifying kinetic model approximations.

An example of the generalized moment of velocity $\boldsymbol{\xi}$, with Cartesian components (u, v, w), is given by $\langle u^p v^q w\rangle$ where (p, q, r) denote selected non-negative integers. The contributions to the evolution of generalized moments due to collisions involve eight dimensional integrals. It can be shown that these integrals may be evaluated using the above equation via algorithmic enumeration of terms resulting from products of multinomials, along with analytical evaluation of elementary integrals. Owing to the adaptive and non-perturbative nature of this approach – unlike other approaches based on Knudsen number expansions – it appears reasonable to speculate that this approach could be capable of predictions over a broader range of Knudsen numbers with consideration of fewer moment constraints.

The potential utility of the adaptive quadrature approach can be demonstrated by investigation of canonical problems, including homogeneous relaxation and shock tube problems. For the case of a homogeneous relaxation, the behavior of the time evolution of velocity variances and covariances, shown in Figure 10, obtained from the quadrature-based approach (based on the full Boltzmann collision integral) is found to be in good agreement with that obtained from DSMC. Although not shown in the figure, evolution of higher order moments are also correctly captured using the quadrature-based approach. Application of the quadrature based approach to a shock tube problem, as shown in Figure 11, indicates that there is a very good agreement between the results based on the Boltzmann collision operator and its BGK approximation at low Knudsen numbers.

3.4 Direct Simulation Monte Carlo

The direct simulation Monte Carlo (DSMC) method is the most widely used technique for numerical modeling of rarefied gas flows, and over the past several decades DSMC has been an important tool in design and analysis for a wide variety of hypersonic flow problems [4]. The DSMC method was initially developed by Bird in the early 1960's for use in simple homogeneous relaxation problems, in which a nonequilibrium gas velocity distribution is driven toward equilibrium by intermolecular collisions [39]. In the decades since, DSMC has been applied with great success to a wide variety of hypersonic engineering problems [40, 41, 42].

While the underlying assumptions in DSMC are valid for any dilute gas flow (i.e. a gas flow for which the collision cross section is much smaller than the spacing between atoms or molecules) the application of DSMC has generally been limited to rarefied flows due to the higher efficiency of continuum CFD techniques for continuum flow simulation. Within the transition Knudsen number regime, DSMC combines a high degree of accuracy, conceptual simplicity, ease of application to complex geometries, and unconditional numerical stability. For high speed rarefied flows, DSMC also tends to be considerably less expensive than other rarefied flow simulation methods, and the applicability of DSMC to complex three-

dimensional flows has increased over time due to continual improvements in available computer resources. Along with development and availability of full-featured DSMC codes [43-47], and particularly the freely available codes of Bird [48], these attributes tend to make DSMC a preferred tool for use in both design and aerothermal analysis of hypersonic vehicles.

3.4.1 Overview of Numerical Procedures

At its core, the DSMC method involves tracking and collision operations among a collection of simulated particles, each representing a large number of atoms or molecules, in a manner which reproduces the underlying physics of the governing Boltzmann equation [4]. In a typical DSMC simulation, every particle is assigned a position, a velocity, a number or pointer to identify the particle species, and internal (rotational and vibrational) energy values. Particles are grouped into finite volume computational cells for use in both collision partner selection and time-averaged sampling of simulation results. Within each cell, the gas density is calculated as a function of the number of particles per unit volume, the gas bulk velocity is the mean velocity of all particles in that cell, and the translational temperature is proportional to the mean-square particle speed in a coordinate frame which moves at the bulk velocity. Rotational and vibrational temperatures – which may differ significantly from the translational temperature in a rarefied hypersonic flow – are computed from the mean internal energy of all particles in the cell. Surface fluxes are calculated from the momentum and energy exchange which occurs as particles are reflected off of solid wall boundaries.

DSMC is an inherently explicit technique, and a DSMC simulation of a steady state flow typically begins with either vacuum or uniform initial conditions. The flowfield then evolves over time toward steady state, after which time-averaged sampling may be performed over a number of time steps to reach desired levels of statistical scatter in the output quantities of interest.

During each simulation time step, a typical DSMC algorithm involves three basic procedures: First, particles are moved through a computational grid according to assigned velocities, and are reassigned as necessary to new cells in this grid. Particles which exit the simulation domain through inflow or outflow boundaries are removed, while any particle which collides with a solid wall boundary is reflected off this boundary according to some gas-surface interaction model. Additional particles may then be introduced along inflow boundaries. Second, particles within each cell are organized into pairs, and collision operations are performed on these pairs in a manner which produces both the desired collision frequency and desired macroscopic transport coefficients. Energy exchange between translational and internal energy modes, as well as chemical reactions, may be applied to some fraction of colliding particles. Finally, if either steady state conditions have been reached or an unsteady flow is being simulated, then sampling routines are used to compile relevant field and surface quantities for output of simulation results.

These basic DSMC procedures, which are performed for every cell during each time step, are outlined in Figure 12. Note that the order of these procedures varies between different implementations of DSMC, and the detailed algorithms and physical models associated with each procedure can vary considerably as well.

3.4.2 Conditions for Accurate Simulation

For accurate DSMC simulation, two numerical criteria must usually be met. First, the time step interval must be small compared to the mean collision time. Second, the mean distance between colliding particles – often termed the “mean collision separation” (MCS) – should be small in relation to the local mean free path (MFP) [4, 48]. The first criterion follows from an operator-splitting approach used to decouple particle movement and collisions during each time step; this criterion is met either by careful limiting of a global time step interval, or by local time step adaptation with different time step intervals employed in different cells. The second criterion, based on a desired MCS/MFP ratio, is often more difficult to meet

without compromising simulation efficiency, and has been the subject of considerable research over the past few decades. Two basic strategies are generally utilized (often together) to limit the MCS in a DSMC simulation: grid adaptation, and reducing grid dependence in the MCS through either adaptive subcells [48] or nearest neighbor collisions [49]. Both strategies are discussed below.

Variation in grid architecture and grid adaptation techniques are arguably the greatest distinguishing characteristics among the different widely used DSMC codes. Unstructured body-fitted grids, as employed in the MONACO DSMC code [44], provide the highest degree of flexibility, but require potentially time-consuming grid generation by the user and can complicate procedures for automatic adaptation to the local mean free path. Most other codes utilize some form of Cartesian grid, with cuboidal or rectangular cells, cut cells along inclined surface boundaries, and capabilities to automatically divide each cell into a number of smaller cells using refinement criteria based on the local mean free path [43, 45, 46]. This strategy avoids requirements to import an externally defined grid, and tends to ease simulation setup for flow problems involving complex surface geometries. Cartesian grid architectures can be further divided into two-level or three-level Cartesian grids, tree structures [50], and multi-element groupings. Other grid types [4], such as a monotonic Lagrangian grid [51], have also been used with some success. Detailed descriptions of the various grid adaptation strategies are provided in the references.

While grid adaptation based on the local mean free path is the most common way to ensure sufficiently small MCS, the MCS can be further reduced by means of subcells or nearest neighbor selection routines. In transient adaptive subcell procedures, all particles in a given cell are organized into smaller subcells as a first step in collision procedures during each time step [48]. Subcell sizes are based on either the local mean free path or the desired number of particles per subcell. Collision partners are then selected from the same subcell if possible; otherwise particles in nearby subcells are paired together. In nearest neighbor selection, the first particle in each collision pair is randomly selected, and the closest particle among all particles in the cell is chosen as the second particle in the pair [49]. Typical modifications to this procedure involve preventing the same two particles from colliding repeatedly, and limiting the nearest neighbor search to some randomly selected subset of all particles in the cell [53, 54].

3.4.3 Collision Procedures

As outlined in Figure 12, DSMC collision procedures include several different steps, and an overview of these steps is provided in the following discussion. In the first step for collision procedures applied to a given cell, some number N_{pairs} of particle pairs are selected from among all particles in the cell. The value of N_{pairs} varies among different collision selection schemes. In the popular "no time counter" (NTC) scheme of Bird [4], N_{pairs} is calculated as

$$N_{pairs} = \frac{1}{2} Nn\left(\sigma c\right)_{\max} \Delta t \tag{25}$$

where N is the number of particles in the cell, n is the time-averaged number density, $(\sigma c)_{\max}$ is the maximum product of collision cross section and relative speed for any collision in the cell over a large number of time steps, and Δt is the time step interval. Each pair is then considered to participate in a collision; using the NTC scheme, a pair is selected if $\sigma_{ij} c_{ij}/(\sigma c)_{\max} > R$, where σ_{ij} and c_{ij} are respectively the collision cross section and relative speed for the (i, j) particle pair, and R is a random number in [0,1]. Other schemes, such as the majorant frequency scheme (MFS) [45] and a scheme of Baganoff and McDonald [52], involve alternate procedures for selecting particles to collide.

In NTC as in other collision selection schemes, collision probabilities are proportional to a collision cross section σ, which is in turn generally a function of the relative incident speed c for the two particles. The dependence of σ on c is directly related to the dependence of transport coefficients – such as viscosity – on

temperature. Most widely used DSMC codes employ the variable hard sphere model [4], for which σ is a power law function of c and viscosity scales with a constant power of translational temperature.

Once colliding pairs have been determined, each pair is considered for probabilistic redistribution of energy between translational and internal energy modes. For any collision involving diatomic or polyatomic molecules, some energy may be exchanged between translational and rotational modes, and the probability of such exchange is equal to the reciprocal of the rotational collision number. This collision number is either set to some constant or is allowed to vary as a function of collision energy or cell-averaged temperature [55]. If translational-rotational energy exchange is determined to have occured, then new particle rotational energies are typically resampled from continuous equilibrium distributions using the technique of Borgnakke and Larsen [56]. For high temperature flow simulations involving vibrational excitation, similar probabilistic procedures are employed to determine whether translational-vibrational energy exchange occurs, and to resample vibrational energy values from quantized equilibrium distributions [4]. For application to very high temperature flows or flows involving gas radiative emission, a similar treatment has been applied to nonequilibrium electronic excitation [4, 57].

Note that commonly used energy exchange procedures [56] are phenomenological, and do not account for potentially important effects such as vibrational-vibrational exchange, anharmonic vibrational quantum levels, and state-dependent exchange probabilities. Although not usually included in DSMC hypersonic flow simulations, all of these phenomena have been considered in a research context [58]. It should be emphasized that the particle nature of DSMC, with individual internal energy values assigned to each particle, provides considerable potential for accurate and efficient simulation of gas flows involving nonequilibrium rotational, vibrational or electronic energy distributions.

For accurate simulation of high enthalpy hypersonic flows, chemistry modeling capabilities are often required. Several DSMC chemistry models have been developed, and of these the total collision energy and vibrationally favored dissociation models are likely in most use [4, 58]. These models are designed to reproduce the temperature dependence of modified Arrhenius reaction rate coefficients, by calculating the reaction probability for a given collision pair as a function of relative translational and internal energies of the colliding particles. Due to the low density in most DSMC applications, chemistry modeling efforts have primarily focused on dissociation and exchange reactions, although some DSMC codes include capabilities for recombination and/or surface catalysis [4]. Recent work of Bird and others has focused on integrated treatment of reactions and vibrational state transitions, with the potential to avoid reliance on near-equilibrium assumptions such as those used in the modified Arrhenius rates [59].

Following any translational-internal energy exchange and chemistry procedures for a given collision pair, the relative translational energy of the two particles is adjusted in order to enforce conservation for the total energy in the collision. Finally, the translational energy is distributed among the two particles in a manner which enforces both energy and momentum conservation [4]. For the standard variable hard sphere (VHS) collision models in a simple (one species) gas, this involves randomly sampling post-collision particle velocities from opposite points on a spherical shell in velocity space, which is centered at the average incident velocity of the two particles. Other collision models employ anisotropic resampling of the post-collision relative velocity, in order to more accurately simulate transport phenomena or other effects [4]. In particular, the variable soft sphere (VSS) model [60] corrects for the inability of the VHS model to independently achieve desired viscosity and mass diffusion rates, and the variable sphere (VS) [61] model simulates the effects of various intermolecular potential functions by fixing the deflection angle between incident and post-collision relative velocities.

3.4.4 Current Research Issues

The DSMC method has advanced considerably in the past several decades, and numerous researchers have made important improvements in accuracy, efficiency and applicability of the method. However, several

research issues remain. Due to advances in computing power, DSMC continues to increase in popularity and become more of a practical tool for complex engineering problems. With the increasing value of DSMC as an engineering tool for hypersonic vehicle design and analysis, a number of research problems have recently received considerable attention, and current DSMC hypersonics research is focused in several different areas. Some of these research areas are cited in the following discussion.

One important set of research topics involves improved characterization of nonequilibrium internal energy distributions, with a particular emphasis on quantized vibrational excitation. In a typical high-enthalpy hypersonic flow, highly nonequilibrium vibrational energy distributions are expected throughout the shock layer and wake, and surface heating, chemical composition and radiative properties may be strong functions of local vibrational energy distributions within these regions. While the traditional DSMC approach [56, 48] to vibrational excitation allows for arbitrary energy distributions, this approach is phenomenological and neglects much of the underlying physical phenomena. Standard DSMC procedures for vibrational excitation involve probabilistic sampling from equilibrium distributions [56], employ a simple harmonic oscillator approximation, and do not consider potentially important processes such as vibrational-vibrational exchange. Vibration-dissociation coupling is also either neglected [4] or greatly simplified [58].

To correct for limitations in traditional DSMC approaches for internal energy exchange, much interest has recently focused on development of state-to-state quantum kinetics models [62], and in new chemistry models which account for the strongly coupled nature of vibrational excitation and chemical reaction mechanisms [59]. Figure 13 illustrates one example, taken from Ref. [62], of the potential accuracy improvements associated with a state-to-state model for vibrational quantum level transitions. The figure shows relative populations at quantum level 4, as a function of transit time through a Mach 7 shock in CO. Results from a traditional DSMC simulation are on the left, while results from a DSMC simulation utilizing a new state-to-state model on the right. (Both DSMC results are shown in red.) In comparing with experimental data points also displayed in Figure 13, we find a substantial improvement in accuracy for the new model during the nonequilibrium relaxation period at small elapsed time values.

Flowfield-radiation coupling is another active area of DSMC research, and effects of shock layer radiation on high enthalpy reentry flowfields may need to be considered for accurate gas flow simulation. Potentially important coupling effects in such flows include spectrally resolved gas emission and absorption, as well as radiation contributions from the vehicle surface and solid particles associated with surface ablation [63, 64]. Radiative emission has been linked to vibrational energy level transitions, and improved characterization of these transitions should allow improved capabilities for estimating both radiative heating for reentry vehicles and plume radiation signatures.

Multiphase rarefied flows are of interest in simulating high altitude solid rocket plumes and spacecraft venting flows, and recent work has focused on development of DSMC models for two-way coupled interaction between a gas and condensed phase particles [65]. Related work has involved model development for nucleation, condensation and evaporation of molecular clusters in freely expanding plumes.

As mentioned above, several different strategies have been employed for DSMC grid adaptation [4], and recent work on multi-level Cartesian grid refinement has shown great promise in effectively adapting grids for complex flowfields [46]. Another newly proposed strategy employs a uniform Cartesian grid with modified collision procedures to reduce cell size dependence in simulation results [66]. The DSMC community is far from a consensus on the most effective grid adaptation technique, and this remains an ongoing research topic.

For efficient and accurate simulation of hypersonic flows involving a wide range of Knudsen number regimes, much recent work has involved development of hybrid schemes which utilize DSMC only in

rarefied regions and apply Navier-Stokes techniques [67, 68, 69] or alternate particle methods [70, 71] over continuum portions of the flowfield. Such hybrid approaches allow DSMC to be employed only within regions where DSMC is relatively efficient and where approximations underlying continuum approaches are assumed to be invalid. Hybrid techniques are particularly useful for simulating low altitude hypersonic flows, where full DSMC simulation may be prohibitively expense but strong local nonequilibrium occurs in the velocity distribution within small flowfield regions. These regions include the bow shock, portions of the boundary layer over leeward surfaces, the area surrounding a sharp leading edge, and low density portions of the wake.

Particular challenges in development of DSMC-based hybrid schemes for simulation of this type of "multi-scale" flow include accurate determination of continuum breakdown for domain decomposition between DSMC and continuum modules of a hybrid code, and communication between the two modules along the continuum breakdown boundary. The gradient length Knudsen number Kn_{max}, given by Eq. (7), is often employed to automatically divide the computational domain between DSMC and continuum regions, with some cutoff value (typically 0.05) used to indicate continuum breakdown. However, accurate assessment of continuum breakdown can require alternate breakdown parameters, and the optimal cutoff value may vary widely between different flows. Several alternate breakdown parameters have been proposed, and characterization of continuum breakdown is currently an active research topic. Communication between DSMC and continuum methods is another area of current research, and is greatly complicated by the potentially large statistical scatter in conserved macroscopic quantities as calculated by DSMC. Approaches to compensate for this scatter include the use of additional DSMC particles within "ghost cells", time-averaging for DSMC quantities [67, 72], and continuum particle methods which are less sensitive to scatter effects than typical Navier-Stokes schemes [70, 71].

Another current DSMC research area of particular importance to rarefied hypersonic flows is gas-surface interaction. The standard Maxwell model for such interactions, which is implemented in most DSMC codes, uses a constant thermal accommodation coefficient (TAC) to specify the probability that any particle-wall boundary collision results in diffuse reflection; otherwise the collision will involve specular reflection [4]. A diffusely reflected particle is assigned new velocity components (and typically new internal energy values as well) which are sampled from distributions corresponding to a stationary gas reservoir at the wall boundary temperature. For a specularly reflected particle, the normal velocity component is reversed while tangential velocity components are unchanged. While the Maxwell model has positive attributes such as simplicity of implementation and availability of TAC values for several surface-gas combinations, the model is very approximate and potentially inaccurate. In particular, this model neglects complex scattering characteristics observed through molecular beam experiments and detailed molecular dynamics simulations. Alternate models, such as the Cercignani-Lampis-Lord (CLL) model [73] add physical realism through the use of additional parameters, but have yet to gain widespread use due to a general lack of knowledge regarding appropriate input parameter values. For realistic treatment of gas-surface interaction, an ideal model would meet several different criteria. These include enforcement of the reciprocity relation [4]; consideration of surface roughness and temperature effects; depends on gas species and surface composition; independent accommodation of internal energy modes; surface catalysis, sublimation and deposition; and scattering distributions which agree well with experimental data. As assumptions and input parameters related to gas-surface interaction may have considerable effects on hypersonic vehicle characteristics – particularly surface heating and aerodynamic forces – additional work in both DSMC model development and experiment seems warranted.

Several other active research areas exist within the DSMC community. These include development of DSMC-based procedures for efficient simulation of subsonic flows [74]; alternate operator splitting schemes for particle advection and collision processes [75]; efficient minimization of the mean collision spacing [53, 54]; analysis of temporal and spatial discretization errors [76]; ionization, electronic excitation and electron transport using either particle or finite volume techniques [77, 78, 79]; time step and numerical weight adaptation [4]; improved modeling of collision dynamics at very low or very high

temperatures [80]; identification of convergence to steady state [81]; and techniques to better utilize computer resources, such as DSMC implementations for graphics processing units, combined use of shared and distributed memory, and improved procedures for parallel domain decomposition [82].

3.4.5 DSMC Simulation Examples

Over the past several decades, the DSMC method has been used extensively in a variety of hypersonic applications. An exhaustive list of these applications is out of the scope of this work, but a number of representative examples are mentioned. These examples are organized under the general categories of aerothermal analysis for atmospheric entry and hypersonic cruise vehicles; and thrusters, plumes and spacecraft aerodynamics. Flows in the first category are distinguished by relatively large aerodynamic drag and heating effects, and vehicle geometries which are primarily designed with aerothermal characteristics in mind. Flows in the second category tend to involve near-free molecular freestream conditions, with the highest gas densities occurring in nearfield plume regions for thrusters or venting sources.

3.4.5.1 Aerothermal Analysis for Atmospheric Entry and Hypersonic Cruise Vehicles

Due to the difficulty and expense of flight experiments involving high Knudsen number flow regimes, most experimental comparisons for assessment of DSMC codes and techniques are based on subscale wind tunnel data. Likely the most comprehensive of these comparisons was promoted by Working Group 18 of the NATO AGARD Fluid Dynamics Panel, and involved wind tunnel tests at four different experimental facilities and extensive comparison among several DSMC and Navier-Stokes codes. A spherically blunted 70° cone, with the same forebody proportions as the Mars Pathfinder aeroshell, was tested under a variety of conditions involving Mach numbers between about 10 and 20. Most test cases used N_2 gas, with sufficiently low freestream enthalpy for negligible dissociation and relatively small vibrational excitation effects. Measured data included surface pressure and heat flux, gas density throughout the flowfield, and normal and axial forces for a range of pitch angles. Rarefaction effects were observed in both the wake and the forebody shock layer, and good overall agreement was generally found between experimental data and DSMC. Study results are reviewed in Ref. [83].

Two examples of comparisons between DSMC and experimental data from the NATO-AGARD study, as taken from Ref. [41], are shown in Figure 14. Contours of normalized density are displayed from axisymmetric MONACO [44] DSMC results and from electron fluorescence measurements of Allegre et al. [84] for a Mach 20.2 case at Kn = 0.03 and 0° angle of attack. Centerline heat flux results are compared for a somewhat higher enthalpy condition at Mach 15.6, Kn = 0.002 and 0° angle of attack. Figure 15 shows pressure and density contours for a case at Mach 20.2, Kn = 0.03 and an angle of attack of 10°. The pressure plot includes surface pressure and scalar field pressure contours as well as streamlines, and was generated from a three dimensional simulation using the newly developed HAP DSMC code [66]. Experimental number density values in Figure 15 are normalized by the local density in an empty test section. Significant asymmetry is observed in both forebody and wake regions due to the angle of attack, and relatively good agreement is found between DSMC and experiment.

In another comprehensive comparison of DSMC and ground test data, a series of axisymmetric hypersonic flows over double cone and cylinder-flare configurations were used to investigate shock-shock and shock-boundary layer interactions under rarefied conditions [85]. Representative results from this study are shown in Figure 16, for a case involving Mach 15.6 flow of nitrogen over a 25°/55° double cone with Kn = 0.002. A plot of pressure contours and streamlines shows extremely complex shock-shock interactions near the junction between the two cones, with a clearly defined recirculating region. Also in Figure 16, experimental data for surface heat flux is compared with simulation results from two different DSMC codes, and very good overall agreement is found. Note the reduction in heat flux around the

recirculation zone, and a heat flux spike where a secondary shock intersects the boundary layer.

As an example of DSMC results for a realistic three dimensional flow over a full scale hypersonic vehicle, Figure 17 shows contours of translational temperature, surface heat flux, Mach number, and streamlines for a Mach 14 flow of air over a viscous-optimized waverider geometry [86] at 0° angle of attack and a simulated altitude of 100 km. The global Knudsen number, based on a body length of 5 m, is 0.02. This simulation was performed using the HAP DSMC code [66], in order to evaluate degradation in waverider lift expected at very high altitudes due to viscous and rarefaction effects. The computed lift-to-drag ratio of about 0.3 was well below that expected at lower altitudes.

Figure 18 shows streamlines and pressure contours from a DSMC simulation of an inflatable "ballute" concept to increase high altitude deceleration during atmospheric reentry, as taken from Moss [87]. Complex shock-shock interactions are found to result from shocks generated around opposite sides of the toroidal ballute, and around the capsule to which the ballute is tethered. In a detailed DSMC study of high altitude ballute aerothermodynamics [87], a variety of flowfield and surface flux characteristics were assessed.

Mach number contours for a Mach 10 flow of nitrogen over a subscale Apollo command module geometry are shown in Figure 19, as taken from DSMC results used in a comparison with aerodynamic coefficients from a series of wind tunnel measurements [88]. Here the Knudsen number is 0.067 and the angle of attack is 30°. Significant discrepancies were observed between DSMC and experimental data for both integrated vehicle drag and pitching moment, although relatively good agreement was found for a slender cone geometry. Excellent agreement was also found between aerodynamic coefficients in Ref. [88] and those calculated using another DSMC code, as discussed in Ref. [41].

Figure 20 shows the surface pressure distribution at an altitude of 400,000 ft for the X-38 vehicle as computed using the DAC DSMC code [40, 43]. The X-38 was designed as a crew return vehicle for the International Space Station, and DSMC simulations were used to evaluate aerodynamic characteristics for reentry conditions between free molecular and continuum flow regimes.

Contours of normalized density for the Space Shuttle Orbiter at 170 km altitude are shown in Fig. 21, as taken from DSMC results of Rault [89]. DSMC simulations were performed for a range of shuttle reentry conditions between 100 km and 170 km altitudes, and DSMC aerodynamic coefficients were compared with flight data, wind tunnel data, and with Navier-Stokes and bridging formula calculations.

In a recent example of the utility of DSMC for hypersonic stability analysis, Abdel-jawad et al. [90] performed a series of DSMC simulations for the ESA Beagle2 vehicle during Mars atmospheric entry, and used simulation results within a vehicle dynamics model to demonstrate static instability. The authors conclude that simple bridging relations, which had been employed in pre-flight analysis to determine the required rate of spin during entry, had underestimated the effect of viscous forces and may have ultimately led to mission failure. Figure 22 shows overall temperature contours from a DSMC simulation used in this study, at an angle of attack of 11° and Kn = 0.0291.

3.4.5.2 Thrusters, Plumes and Spacecraft Aerodynamics

In addition to hypersonics applications involving high altitude aircraft and reentry vehicles, common DSMC applications include exo-atmospheric plume impingement analysis and satellite aerodynamics. One such example is the extensive use of the SMILE DSMC code [45] for transition regime analysis of the Mir space station during atmospheric descent, prior to its controlled deorbit in 2001 [91]. DSMC simulation results likely assisted in decisions regarding the descent trajectory and orientation. Figure 23 shows streamlines around Mir from SMILE calculations for a simulated altitude of 110 km.

Figure 24 shows the surface pressure distribution on Mir due to Space Shuttle Reaction Control System (RCS) exhaust gases [40], as part of simulations using the DAC DSMC code [43] in support of a planned Space Shuttle docking. DSMC simulations provided detailed information on plume impingement effects associated with various RCS thruster combinations.

Simulations of high altitude and exo-atmospheric rocket exhaust plumes have often involved an uncoupled two-step approach. In this approach, a Navier-Stokes CFD code is employed efficient simulation of continuum nearfield plume regions (possibly including portions of the nozzle), and a continuum breakdown surface within the Navier-Stokes domain is then used as an inflow boundary for a subsequent DSMC simulation. DSMC inflow boundary conditions are based on Navier-Stokes simulation results along the breakdown surface, and an accurate solution is assumed if the bulk flow is uniformly supersonic in the surface-normal direction and directed into the DSMC domain. This approach was used to generate the pressure distribution in Figure 24. Figure 25 shows centerline density contours from another example of this approach, also involving the DAC code [43], for which interacting plumes are simulated from simultaneous firings of three Space Shuttle RCS thrusters [40]. Black lines in Figure 25 indicate inflow boundaries used in the DSMC simulation, and nearfield plume results within the regions enclosed by these lines are from an uncoupled Navier-Stokes simulation. Note the complex farfield plume interactions shown in the figure, with a high-density mixing layer bounded on both sides by oblique shocks. The placement of DSMC inflow boundaries along continuum breakdown surfaces in this type of flow problem is further illustrated in Figure 26. This figure shows a breakdown surface in green, based on calculation of Bird's expansion flow parameter [4] from Navier-Stokes simulation results, for a generic rocket exhaust plume at high altitude [92]. The Blue surface in Figure 26 is a smoothed approximation of the continuum breakdown surface, and is employed as a nonuniform inflow boundary for a DSMC simulation.

Figure 27 shows contours of surface pressure from a DSMC simulation of plume impingement on the Hubble Space Telescope, due to Space Shuttle airlock venting during a planned servicing mission [40]. Following unanticipated effects of airlock venting during a previous Hubble servicing mission, extensive DSMC-based analysis was performed as part of mission preparation. The Space Shuttle payload bay, airlock and cargo, shown in Figure 27, were also included in the simulations.

Figure 28, also taken from DSMC results in Ref. [40], shows the surface heat flux distribution over the Mars Global Surveyor during a planned aerobraking maneuver in the upper atmosphere of Mars [93]. This mission constituted the first use of aerobraking as the primary means of orbit adjustment, and DSMC simulations played an important role in mission planning. As discussed in Ref. [93], DSMC was also used extensively for post-launch aerothermal analysis, following an unplanned change in aerobraking configuration due to an unlatched solar panel.

4.0 SUMMARY

A general overview of rarefied effects in hypersonic flows has been presented, with emphasis on numerical modeling, relevant applications and critical research issues. Phenomena associated with rarefied hypersonic and high enthalpy gas flows was described, including both translational and internal energy nonequilibrium. An overview was provided for several different techniques used to simulate rarefied gas flows, and representative examples were discussed for various techniques. The direct simulation Monte Carlo (DSMC) method, which is the most commonly used simulation method for high Mach number rarefied flows, has been described in particular detail. A number of DSMC examples were presented, including detailed comparisons with experimental data and three dimensional simulations of complex engineering problems related to the Space Shuttle, Mir and other spacecraft and atmospheric entry vehicles. For DSMC, as for discrete velocity Boltzmann and other methods, various shortcomings, recent developments and areas of current research were discussed.

While any brief discussion of such a broad range of topics is necessarily incomplete, it is hoped that the material presented here can serve as a general introduction to a range of techniques and issues associated with simulation of nonequilibrium hypersonic flows. It should be emphasized that material discussed here represents only a small sample of the extensive work in rarefied gas simulation over the past several decades, and the references provide far more detail on much of this work.

5.0 ACKNOWLEDGMENTS

The authors would like to thank Prakash Vedula at the University of Oklahoma for contributing the section on moment methods, and Iain Boyd at the University of Michigan for providing helpful materials related to the content and format of this paper.

6.0 REFERENCES

[1] Talbot, L., *Rarefied Gas Dynamics*, Academic Press, New York, 1960.
[2] Muntz, E. P., Weaver, E. P., and Campbell, D. H., *Rarefied Gas Dynamics: Space Related Studies*, AIAA, Washington D.C., 1989.
[3] Bird, G. A., "Breakdown of Translational and Rotational Equilibrium in Gasesous Expansions," *AIAA Journal*, Vol. 8, 1970, pp. 1997-2003.
[4] Bird, G. A., *Molecular Gas Dynamics and the Direct Simulation of Gas Flows*, Clarendon Press, Oxford, 1994.
[5] Boyd, I. D., "Predicting the Breakdown of the Continuum Equations under Rarefied Flow Conditions," *Rarefied Gas Dynamics, 23rd International Symposium*, American Institute of Physics, 2003.
[6] Sun, Q., and Boyd, I. D., "A Direct Simulation Method for Subsonic Microscale Gas Flows," *Journal of Computational Physics*, Vol. 179, 2002, pp. 400-425.
[7] Chapman, S., and Cowling, T. G., *The Mathematical Theory of Non-Uniform Gases*, Cambridge University Press, London, 1970.
[8] Vincenti, W. G., and Kruger, C. H., *Introduction to Physical Gas Dynamics*, John Wiley and Sons, New York, 1967.
[9] Boyd, I. D., Chen, G., and Candler, G. V., "Predicting the Failure of the Continuum Fluid Equations in Transitional Hypersonic Flows," *Physics of Fluids*, Vol. 7, 1995, pp. 210-219.
[10] Sun, W., Wang, Q., and Boyd, I. D., "Towards Development of a Hybrid DSMC-CFD Method for Simulating Hypersonic Interacting Flows," AIAA Paper 2002-3099, 2002.
[11] Anderson, J. D., *Hypersonic and High Temperature Gas Dynamics*, 2nd Edition, AIAA Education Series, Reston, Virginia, 2006.
[12] Capitelli, M., Ed., *Nonequilibrium Vibrational Kinetics*, Springer-Verlag, Berlin, 1986.
[13] Chernyi, G. G., Losev, S. A., Macheret, S. O., and Potapkin, B. V., *Physical and Chemical Processes in Gas Dynamics: Cross Sections and Rate Constants*, Vol. 1-2, AIAA Progress Series in Astronautics and Aeronautics, Reston, Virginia, 2002, 2004.
[14] Rich, J. W., Macheret, S. O., and Adamovich, I. V., "Aerothermodynamics of Vibrationally Excited Gases," *Experimental Thermal and Fluid Science*, Vol. 13, No. 1, 1996, pp. 1-10.
[15] Adamovich, I. V., Macheret, S. O., Rich, J. W., and Treanor, C. E., "Vibrational Relaxation and Dissociation Behind Shock Waves Part 1: Kinetic Rate Models, Part2: Master Equation Modeling," *AIAA Journal*, Vol. 33, No. 6, 1995.
[16] Josyula, E., Bailey, W. F., and Ruffin, S. F., "Reactive and Nonreactive Vibrational Energy Exchanges in Nonequilibrium Hypersonic Flows," *Physics of Fluids*, Vol. 15, No. 10, 2003, pp. 3223-3235.
[17] Treanor, C. E., Rich, I. W., and Rehm, R. G., "Vibrational Relaxation of Anharmonic Oscillators with Exchange-Dominated Collisions," *Journal of Chemical Physics*, Vol. 48, 1968, pp. 1798-1807.
[18] Capitelli, M., Gorse, C., and Billing, G. D., "VV Up-Pumping in Nonequilibrium Nitrogen: Effects

on the Dissociation Rate," *Chemical Physics*, Vol. 52, No. 3, 1980, pp. 299-304.
[19] Billing, G. D., and Fisher, E. R., "VV and VT Rate Coefficients in Diatomic Nitrogen by a Quantum Classical Model," *Chemical Physics*, Vol. 43, No. 3, 1979, pp. 395-401.
[20] Schwartz, R. N., Slawsky, Z. I., and Herzfeld, K. F., "Calculation of Vibrational Relaxation Times in Gases," *Journal of Chemical Physics*, Vol. 20, No. 10, 1952, pp. 1591-1599.
[21] Josyula, E., Aliat, A., and Vedula, P., "Multiquantum State-to-State Transitions in Hypersonic Blunt Body Flows," AIAA Paper 2011-532, 2011.
[22] Adamovich, I. V., and Rich, J. W., "Three-Dimensional Non-Perturbative Analytic Model of Vibrational Energy Transfer in Atom-Molecule Collisions," *Journal of Chemical Physics*, Vol. 109, No. 18, 1998, pp. 7711-7724.
[23] Nikitin, E., and Osipov, A., *Kinetics and Catalysis*, VINITI, All Union Institute of Scientific and Technical Information, Moscow, 1977.
[24] Cecignani, C., *Rarefied Gas Dynamics: From Basic Concepts to Actual Calculations*, Cambridge University Press, New York, 2000.
[25] Tcheremissine, F. G., "Solution of the Boltzmann Kinetic Equation for High-Speed Flows," *Computational Mathematics and Mathematical Physics*, Vol. 46, No. 2, 2006, pp. 315–329.
[26] Burt, J. M., Deschenes, T. R., Boyd, I. D., and Josyula, E., "Evaluation of a Hybrid Boltzmann-Continuum Method for High Speed Nonequilibrium Flows," AIAA Paper 2010-1569, 2010.
[27] Kolobov, V. I., Arslanbekov, R. R., Aristov, V. V., Frolova, A. A., and Zabelok, S. A., "Unified Solver for Rarefied and Continuum Flows with Adaptive Mesh and Algorithm Refinement," *Journal of Computational Physics*, Vol. 223, 2007, pp. 589-608.
[28] Josyula, E., Arslanbekov, R. R., Kolobov, V. I., and Gimelshein, S. F., "Evaluation of Kinetic/Continuum Solver for Hypersonic Nozzle-Plume Flow," *Journal of Spacecraft and Rockets*, Vol. 45, No. 4, 2008, pp. 665-676.
[29] Arslanbekov, R. R., Kolobov, V. I., Frolova, A., Zabelok, S., and Josyula, E., "Evaluation of a Unified Kinetic/Continuum Solver for Computing Heat Flux in Hypersonic Blunt Body Flows," AIAA Paper 2007-4544, 2007.
[30] Bhatnagar, P. L., Gross. E. P., and Krook, M., "A Model for Collision Processes in Gases. I. Small Amplitude Processes in Charged and Neutral One Component Systems," *Physical Review*, Vol. 94, No. 3, 1954, pp. 511-525.
[31] Xu, K., "A Gas-Kinetic BGK Scheme for the Navier-Stokes Equations and its Connection with Artificial Dissipation and Godunov Method," *Journal of Computational Physics*, Vol. 171, 2001, pp. 289–335.
[32] Xu, K., and Josyula, E., "Multiple Translational Temperature Model and its Shock Structure Solution," *Physical Review E*, Vol. 71, 2005, 056308.
[33] Ohwada, T., "Structure of Normal Shock Waves: Direct Numerical Analysis of the Boltzmann Equation for Hard-Sphere Molecules," *Physics of Fluids A*, Vol. 5, No. 1, 1993, pp. 271–234.
[34] Hilbert, D., *Grundzüge einer allgemeinen Theorie der linearen Integralgleichungen*, Chelsea Publishing Company, New York, 1953, p. 267.
[35] Chapman, S., "On the Law of Distribution of Molecular Velocities, and on the Theory of Viscosity and Thermal Conduction, in a Non-uniform Simple Monatomic Gas," *Philosophical Transactions of the Royal Society A*, Vol. 216, 1916.
[36] Chapman, S., "On the Kinetic Theory of a Gas. Part II. A Composite Monatomic Gas: Diffusion, Viscosity, and Thermal Conduction," *Philosophical Transactions of the Royal Society A*, Vol. 217, 1918, pp 115-197.
[37] Enskog, D., *Kinetische theorie der vorgange in massig verdunnten gasen. I. Allgeimeiner Teil*, Almqvist and Wiksell, Uppsala, Sweden, 1917.
[38] Grad, H., "On the Theory of Rarefied Gases," *Communications on Pure and Applied Mathematics*, Vol. 2, No. 4, 1949. pp. 331-407.
[39] Bird, G. A., "Approach to Translational Equilibrium in a Rigid Sphere Gas," *Physics of Fluids*, Vol. 6, 1963, pp. 1518-1519.
[40] LeBeau, G. J., and Lumpkin, F. E., "Application Highlights of the DSMC Analysis Code (DAC)

Software for Simulating Rarefied Flows," *Computer Methods in Applied Mechanics and Engineering*, Vol. 191, 2001, pp. 595-609.
[41] Boyd, I. D., "Direct Simulation Monte Carlo for Atmospheric Entry Part II: Code Development and Application Results," in *Hypersonic Entry and Cruise Vehicles*, von Karman Institute for Fluid Dynamics, Rhode-Saint-Genese, Belgium, 2008.
[42] Oran, E. S., Oh, C. K., and Cybyk, B. Z., "Direct Simulation Monte Carlo: Recent Advances and Applications," *Annual Review of Fluid Mechanics*, Vol. 30, 1998, pp. 403-441.
[43] LeBeau, G. J., "A Parallel Implementation of the Direct Simulation Monte Carlo Method," *Computer Methods in Applied Mechanics and Engineering*, Vol. 174, 1999, pp. 319-337.
[44] Dietrich, S., and Boyd, I. D., "Scalar and Parallel Optimized Implementation of the Direct Simulation Monte Carlo Method," *Journal of Computational Physics*, Vol. 126, 1996, pp. 328-342.
[45] Ivanov, M. S., Markelov, G. N., and Gimelshein, S. F., "Statistical Simulation of Reactive Rarefied Flows: Numerical Approach and Applications," AIAA Paper 98-2669, 1998.
[46] Gao, D., Zhang, C., and Schwartzentruber, T. E., "A Three-Level Cartesian Geometry Based Implementation of the DSMC Method," AIAA Paper 2010-450, 2010.
[47] Wu, J.-S., Tseng, K.-C., and Wu, F.-Y., "Parallel Three-Dimensional DSMC Method Using Mesh Refinement and Variable Time-step Scheme," *Computer Physics Communications*, Vol. 162, 2004, pp. 166-187.
[48] Bird, G. A., "The DS2V/3V Program Suite for DSMC Calculations," *Rarefied Gas Dynamics, 24th International Symposium*, American Institute of Physics, Vol. 762, 2005, pp. 541-546.
[49] LeBeau, G. J., Boyles, K. A., and Lumpkin, F. E., "Virtual Sub-cells for the Direct Simulation Monte Carlo Method," AIAA Paper 2003-1031, 2003.
[50] Olson, S. E., and Christlieb, A. J., "Gridless DSMC," *Journal of Computational Physics*, Vol. 227, 2008, pp. 8035-8064.
[51] Oh, C. K., Sinkovits, R. S., Cybyk, B. Z., Oran, E. S., and Boris, J. P., "Parallelization of Direct Simulation Monte Carlo Method with Monotonic Lagrangian Grid," *AIAA Journal*, Vol. 34, No. 7, 1996, 1363-1370.
[52] Baganoff, D., and McDonald, J. D., "A Collision-Selection Rule for a Particle Simulation Method Suited to Vector Computers," *Physics of Fluids A*, Vol. 2, No. 7, 1990, pp. 1248-1259.
[53] Macrossan, M. N., "Searching for a Near Neighbor Particle in DSMC Cells Using Pseudo-Subcells," *Journal of Computational Physics*, Vol. 229, 2010, pp. 5857-5861.
[54] Gallis, M. A., and Torczynski, J. R., "Effect of Collision-Partner Selection Schemes on the Accuracy and Efficiency of the Direct Simulation Monte Carlo Method," *International Journal for Numerical Methods in Fluids*, 2010 (published online; DOI: 10.1002/fld.2409).
[55] Boyd, I. D., "Analysis of Rotational Nonequilibrium in Standing Shock Waves of Nitrogen, *AIAA Journal*, Vol. 28, 1990, pp. 1997-1999.
[56] Borgnakke, C., and Larsen, P. S., "Statistical Collision Model for Monte Carlo Simulation of Polyatomic Gas Mixture," *Journal of Computational Physics*, Vol. 18, 1975, pp. 405-420.
[57] Carlson, A. B., and Hassan, H. A., "Direct Simulation of Re-Entry Flows with Ionization," *Journal of Thermophysics and Heat Transfer*, Vol. 6, No. 3, 1992, pp. 400-404.
[58] Boyd, I. D., "Nonequilibrium Chemistry Modeling in Rarefied Hypersonic Flows," *Chemical Dynamics in Extreme Environments*, World Scientific Press, Singapore, 2001, pp. 81-137.
[59] Gallis, M. A., Bond, R. B., and Torczynski, J. R., "A Kinetic-Theory Approach for Computing Chemical-Reaction Rates in Upper-Atmosphere Hypersonic Flows," *Journal of Chemical Physics*, Vol. 131, 2009, 124311.
[60] Koura, K., and Matsumoto, H., "Variable Soft Sphere Molecular Model for Air Species," *Physics of Fluids A*, Vol. 4, 1992, pp. 1083-1085.
[61] Matsumoto, H., "Variable Sphere Molecular Model for Inverse Power Law and Lennard-Jones Potentials in Monte Carlo Simulations," *Physics of Fluids*, Vol. 14, No. 12, 2002, pp. 4256-4265.
[62] Boyd, I. D., and Josyula, E., "State Resolved Vibrational Relaxation Behind Strong Shock Waves," AIAA Paper 2011-0448, 2011.
[63] Gallis, M. A., and Harvey, J. K., "Atomic Species Radiation from Air Modeled Using the Direct

Simulation Monte Carlo Method," *Journal of Thermophysics and Heat Transfer*, Vol. 9, 1995, pp. 456-463.
[64] Ozawa, T., Levin, D. A., Wang, A., and Modest, M., "Development of Coupled Particle Hypersonic Flowfield-Photon Monte Carlo Radiation Methods," *Journal of Thermophysics and Heat Transfer*, Vol. 24, No. 3, 2010, pp. 612-622.
[65] Burt, J. M., and Boyd, I. D., "High-Altitude Plume Simulations for a Solid Propellant Rocket," *AIAA Journal*, Vol. 45, No. 12, 2007, pp. 2872-2884.
[66] Burt, J. M., Josyula, E., and Boyd, I. D., "A Novel Cartesian Implementation of the Direct Simulation Monte Carlo Method," AIAA Paper 2011-632, 2011.
[67] Schwartzentruber, T. E., and Boyd, I. D., "A Modular Particle-Continuum Numerical Method for Hypersonic Non-equilibrium Gas Flows," *Journal of Computational Physics*, Vol. 225, 2007, pp. 1159-1174.
[68] Lian, Y.-Y., Wu, J.-S., Cheng, G., and Koomullil, R., "Development of a Parallel Hybrid Method for the DSMC and NS Solver," AIAA Paper 2005-0435, 2005.
[69] Garcia, A. L., Bell, J. B., Crutchfield, W. Y., and Alder, B. J., "Adaptive Mesh and Algorithm Refinement Using Direct Simulation Monte Carlo," *Journal of Computational Physics*, Vol. 154, 1999, pp. 134-155.
[70] Burt, J. M., and Boyd, I. D., "Extension of a Multiscale Particle Scheme to Near-Equilibrium Viscous Flows," *AIAA Journal*, Vol. 47, No. 6, 2009, pp. 1507-1517.
[71] Macrossan, M. N., "A Particle-Only Hybrid Method for Near-Continuum Flows," *Rarefied Gas Dynamics: 22nd International Symposium*, American Institute of Physics, 2001, pp. 388-395.
[72] Sun, Q., and Boyd, I. D., "Evaluation of Macroscopic Properties in the Direct Simulation Monte Carlo Method," *Journal of Thermophysics and Heat Transfer*, Vol. 19, No. 3, 2005, pp. 329-335.
[73] Lord, R. G., "Some Extensions to the Cercignani-Lampis Gas Scattering Kernel," *Physics of Fluids A*, Vol. 3, 1991, pp. 706-710.
[74] Homolle, T. M. M., Hadjiconstantinou, "A Low-Variance Deviational Simulation Monte Carlo for the Boltzmann Equation," *Journal of Computational Physics*, Vol. 226, 2007, pp. 2341-2358.
[75] Bird, G. A., Gallis, M. A., Torczynski, J. R., and Rader, D. J., "Accuracy and Efficiency of the Sophisticated Direct Simulation Monte Carlo Algorithm for Simulating Noncontinuum Gas Flows," *Physics of Fluids*, Vol. 21, 2009, 017103.
[76] Gallis, M. A., Torczynski, J. R., and Rader, D. J., "DSMC Convergence Behavior for Transient Flows," AIAA Paper 2007-4258, 2007.
[77] Carlson, A. B., and Hassan, H. A., "Direct Simulation of Re-entry Flows With Ionization," *Journal of Thermophysics and Heat Transfer*, Vol. 6, 1992, pp. 400-404.
[78] Liechty, D. S., and Lewis, M., "Treatment of Electronic Energy Level Transition and Ionization Following the Particle-Based Chemistry Model," AIAA Paper 2010-449, 2010.
[79] Boyd, I. D., "Modeling of Associative Ionization Reactions in Hypersonic Rarefied Flows," *Physics of Fluids*, Vol. 19, 2007, 096102.
[80] Macrossan, M. N., and Lilley, C. R., "Modified Generalized Hard Sphere Collision Model for Direct Simulation Monte Carlo Calculations," *Journal of Thermophysics and Heat Transfer*, Vol. 17, No. 2, 2003, pp. 289-291.
[81] Burt, J. M., and Boyd, I. D., "A Global Convergence Criterion for Steady State DSMC Simulations," *Rarefied Gas Dynamics, 27th International Symposium*, American Institute of Physics, 2011 (to appear).
[82] Schwartzentruber, T., and Gao, D., "Parallel Implementation of the Direct Simulation Monte Carlo Method For Shared Memory Architectures," AIAA Paper 2010-451, 2010.
[83] Moss, J. N., and Price, J. M., "Survey of Blunt Body Flows Including Wakes at Hypersonic Low-Density Conditions," *Journal of Thermophysics and Heat Transfer*, Vol. 11, 1997, pp. 321-329.
[84] Allegre, J., Bisch, D., and Lengrand, J. C., "Experimental Rarefied Density Flowfields at Hypersonic Conditions Over 70-Degree Blunted Cone," *Journal of Spacecraft and Rockets*, Vol. 34, No. 6, 1997, pp. 714-718.
[85] Moss, J. N., and Bird, G. A., "Direct Simulation Monte Carlo Simulations of Hypersonic Flows With

Shock Interactions," *AIAA Journal*, Vol. 43, No. 12, 2005, pp. 2565-2573.
[86] Drayna, T. W., Nompelis, I., and Candler, G. V., "Numerical Simulation of the AEDC Waverider at Mach 8," AIAA Paper 2006-2816, 2006.
[87] Moss, J. N., "Direct Simulation Monte Carlo Simulations of Ballute Aerothermodynamics Under Hypersonic Rarefied Conditions," *Journal of Spacecraft and Rockets*, Vol. 44, No. 2, 2007, pp. 289-298.
[88] Padilla, J. F., and Boyd, I. D., "Assessment of Rarefied Hypersonic Aerodynamics Modeling and Windtunnel Data," AIAA Paper 2006-3390, 2006.
[89] Rault, D. F. G., "Aerodynamics of the Shuttle Orbiter at High Altitudes," *Journal of Spacecraft and Rockets*, Vol. 31, No. 6, 1994, pp. 944-952.
[90] Abdel-jawad, M. M., Goldsworthy, M. J., and Macrossan, M. N., "Stability Analysis of Beagle2 in Free-Molecular and Transition Regimes," Journal of Spacecraft and Rockets, Vol. 45, No. 6, 2008, pp. 1207-1212.
[91] Markelov, G. N., Kashkovsky, A. V., and Ivanov, M. S., "Space Station Mir Aerodynamics Along the Descent Trajectory," *Journal of Spacecraft and Rockets*, Vol. 38, No. 1, 2001, pp. 43-50.
[92] VanGilder, D. B., Chartrand, C. C., Papp, J., Wilmoth, R., and Sinha, N., "Computational Modeling of Nearfield to Farfield Plume Expansion," AIAA Paper 2007-5704, 2007.
[93] Wilmoth, R. G., Rault, D. F. G., Cheatwood, F. M., Engelund, W. C., and Shane, R. W., "Rarefied Aerothermodynamic Predictions for Mars Global Surveyor, *Journal of Spacecraft and Rockets*, Vol. 36, No. 3, 1999, pp. 314-322.

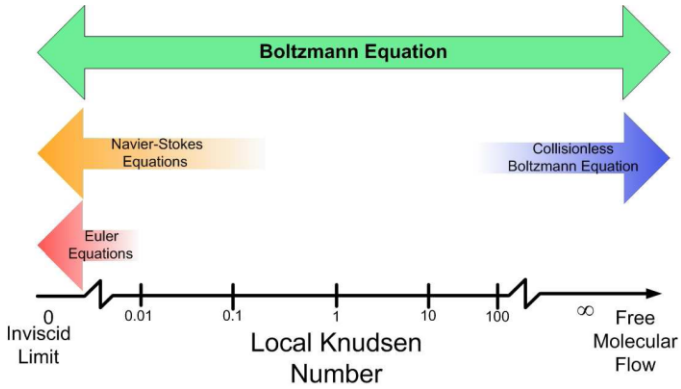

Figure 1: Validity range of different transport equations.

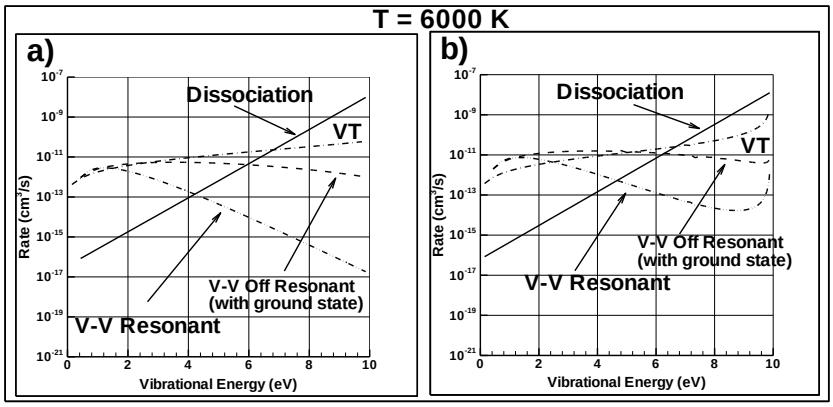

Figure 2: Population weighted transition rates of reactive and non-reactive energy exchanges in N_2 dissociation at 6000 K; (a) Rate set 1 [18, 19], (b) Rate set 2 (SSH rates) [20].

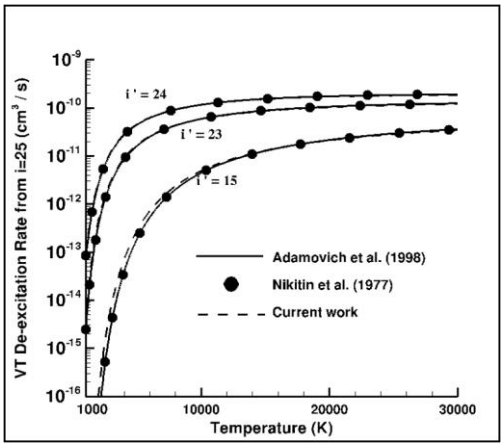

Figure 3: Variation of single and multiquantum rates for $N_2(i=25)+N_2 \rightarrow N_2(i'=15,23,24)+N_2$ [21, 22, 23].

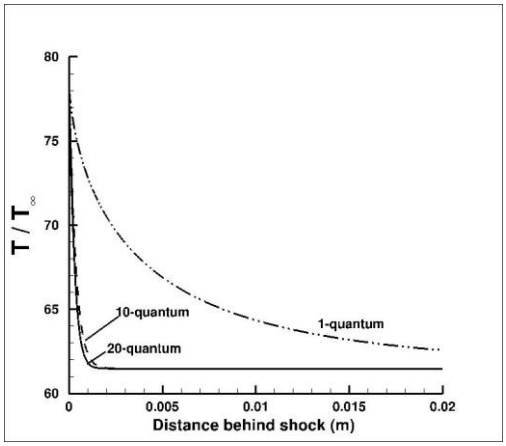

Figure 4: Translational temperature behind shock wave for single and multiquantum VT rates, Mach 19.82 nitrogen flow, 27 Pa, 300 K.

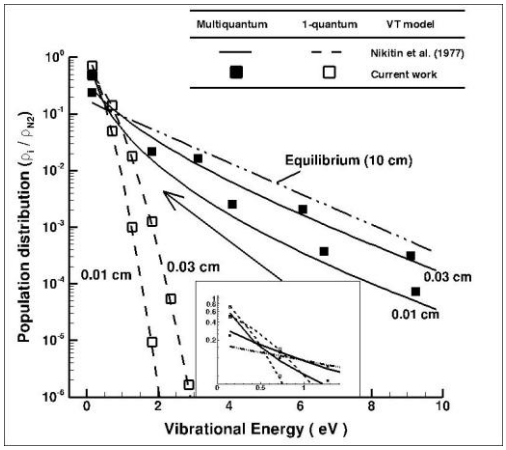

Figure 5: Population distributions behind shock wave for single and multiquantum VT rates, Mach 19.82 nitrogen flow, 27 Pa, 300 K.

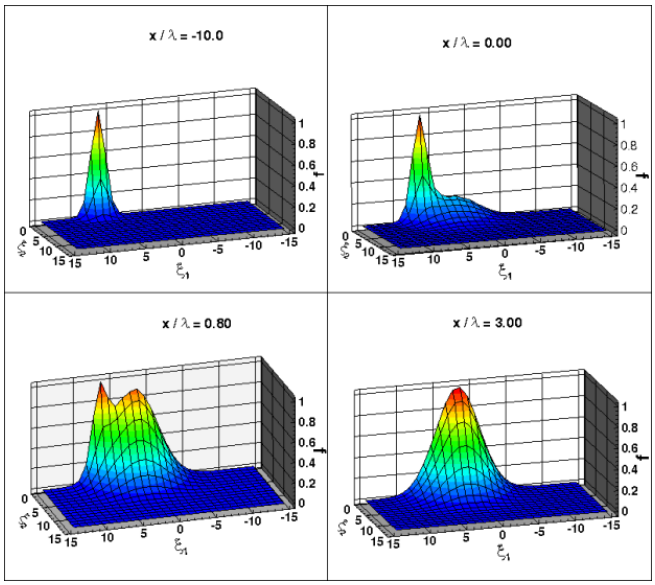

Figure 6: Velocity distribution function inside a Mach 5 shock wave with hard sphere collision model, (a) x/λ = -10, (b) x/λ = 0, (c) x/λ = 0.8, (d) x/λ = 3.

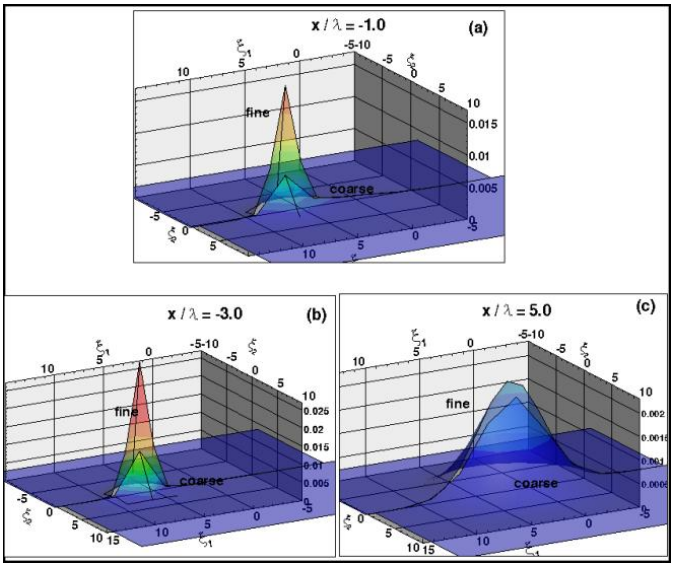

Figure 7: Velocity grid resolution: Probability distribution function in a Mach 5 shock wave with hard sphere collision model on coarse and fine grids, (a) x/λ = -1, x/λ = -3, (c) x/λ = 5.

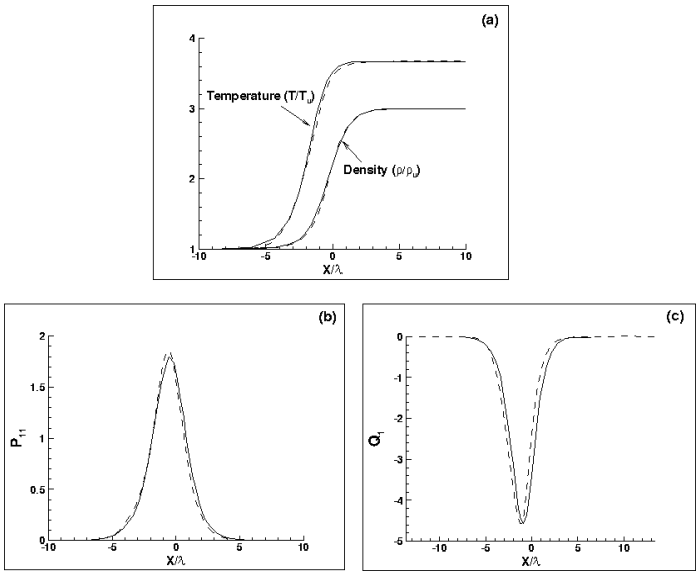

Figure 8: Accuracy of gas kinetic scheme: Macroscopic parameters inside a Mach 3 shock wave with hard sphere collision model, (a) density and temperature, (b) viscous stress xx-component, (c) heat flux x-component.
– – – – – Gas Kinetic Scheme ——— Boltzmann [33]

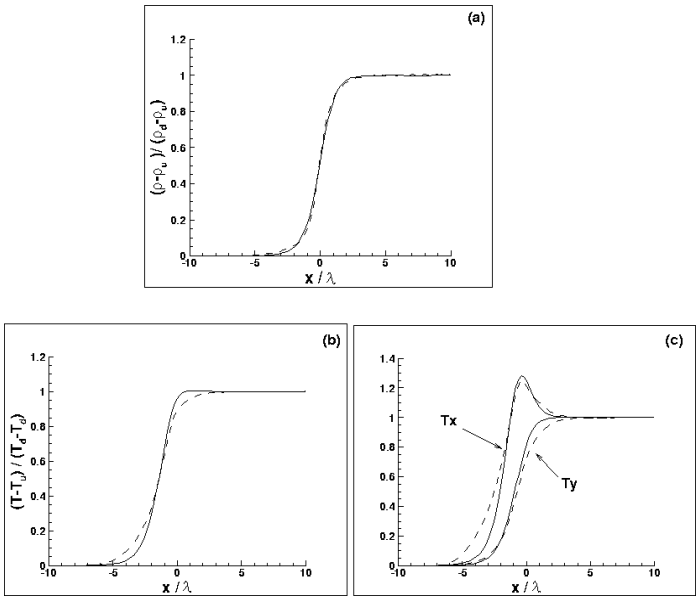

Figure 9: Accuracy of gas kinetic scheme: Macroscopic parameters inside a Mach 5 shock wave with hard sphere collision model, (a) density, (b) temperature, (c) streamwise and normal components of temperature. – – – – – Gas Kinetic Scheme ——— Boltzmann [33]

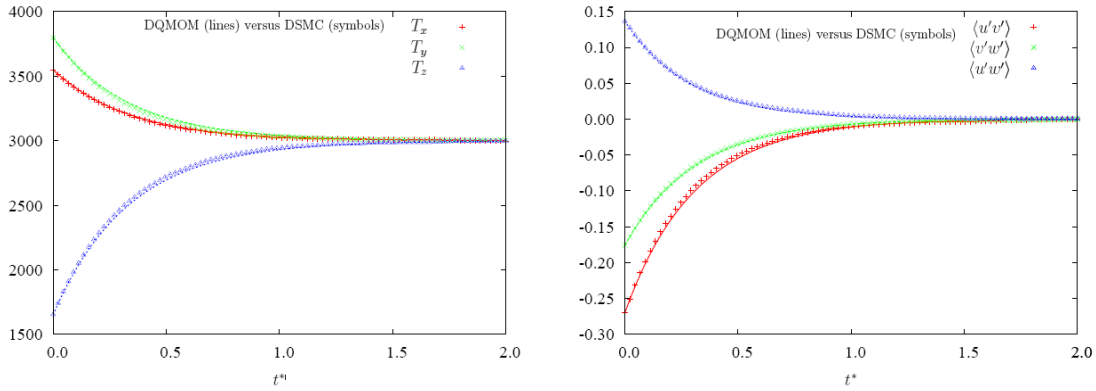

Figure 10: Time evolution of translational temperature components (or measures of velocity component variances) (left figure) and velocity component covariances (right figure) for a single species undergoing homogeneous translational relaxation. Comparison shows good agreement between quadrature-based approach and DSMC.

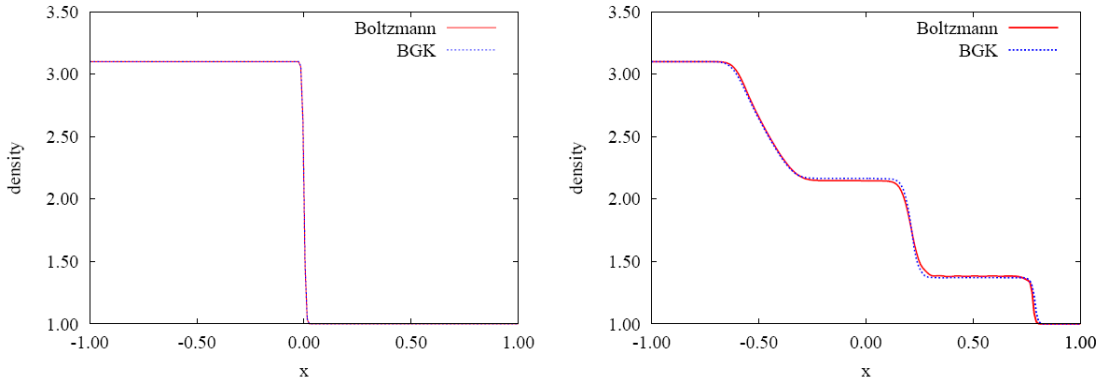

Figure 11: Comparison of density profiles predicted by collisional Boltzmann equation and BGK model in a 1D shock tube, at *t* = 0 (left) and t = 0.5 (right).

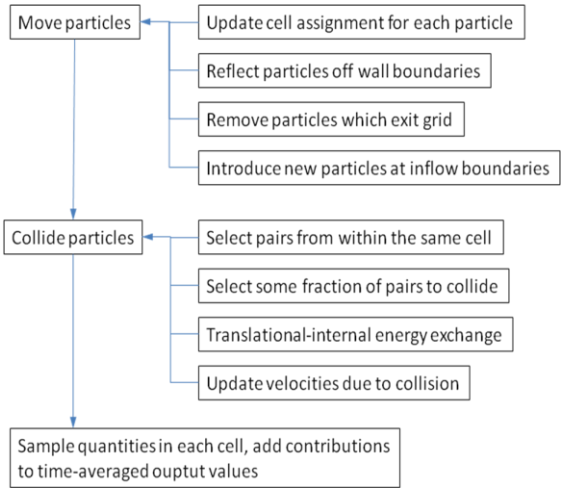

Figure 12: Flowchart for DSMC simulation procedures during each time step.

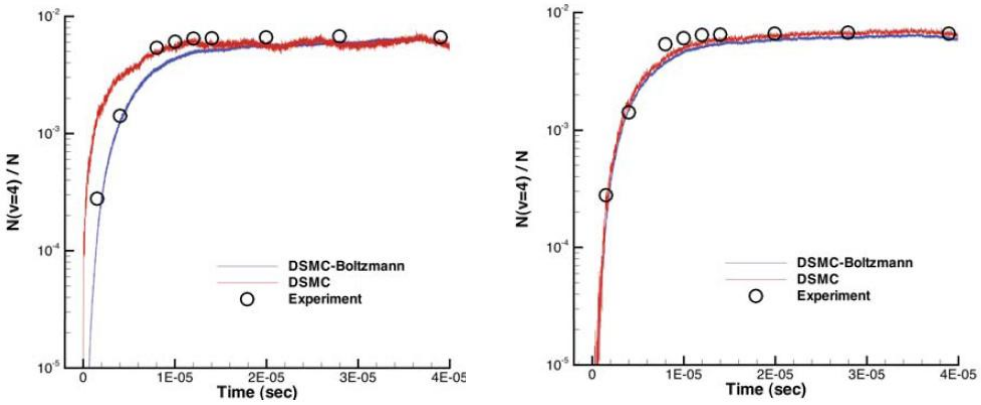

Figure 13: Variation in the relative population of CO at vibrational quantum level 4 as a function of transit time through a Mach 7 shock wave. Red line on left shows traditional DSMC result; red line on right shows result using state resolved energy exchange procedure [62].

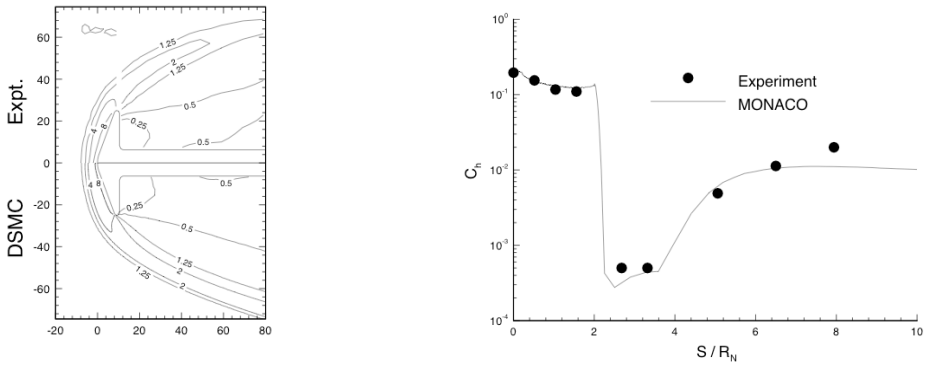

Figure 14: Comparison of normalized density (left) and surface heat flux coefficient (right) between MONACO DSMC and experiment for hypersonic flows over a blunted 70° cone at 0° angle of attack [41]. Density is for Mach 20.2, Kn = 0.03; heat flux is for Mach 15.6, Kn = 0.002.

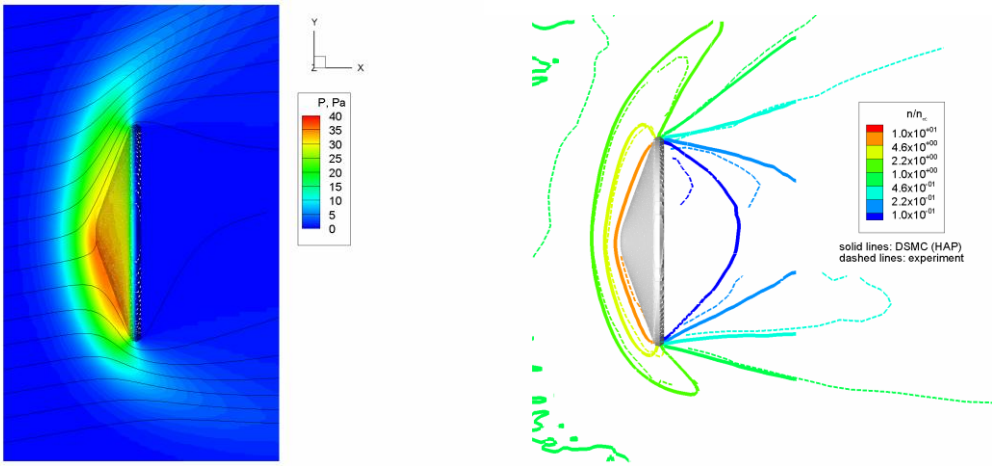

Figure 15: Pressure contours and streamlines (left), and comparison of DSMC and experimental data for normalized density (right) for Mach 20.2 flow of N_2 over a blunted 70° cone at 10° angle of attack, with Kn = 0.03 [66].

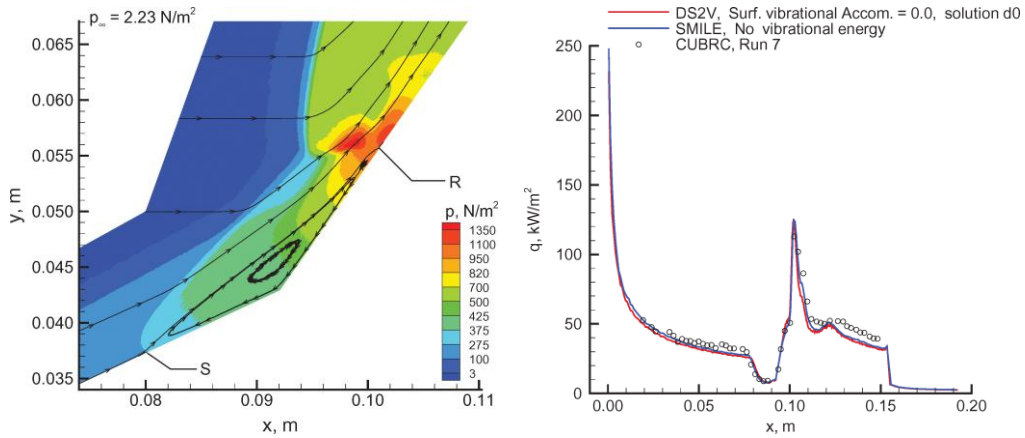

Figure 16: Pressure contours and streamlines (left), comparison of DSMC and experimental heat flux values (right) for Mach 15.6 flow over double cone, with Kn = 0.002 [85].

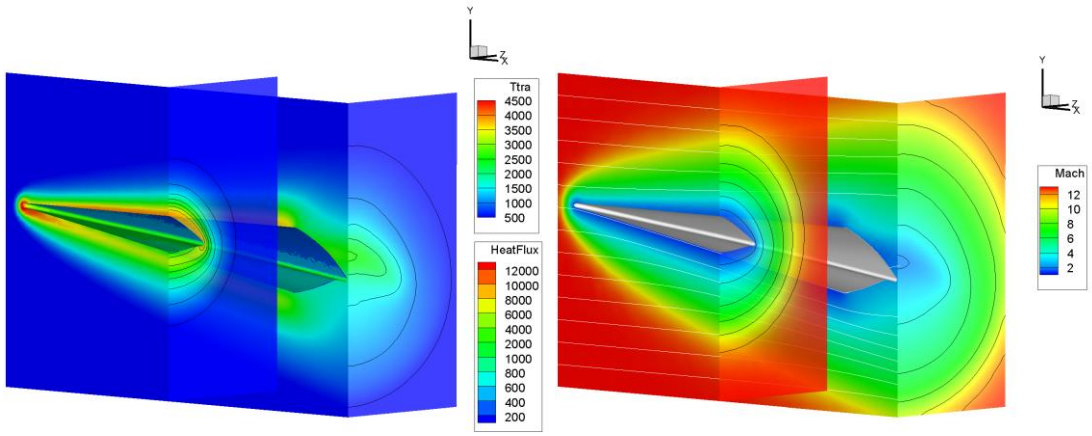

Figure 17: Translational temperature, surface heat flux (left, in K and W/m^2 respectively), Mach number and streamlines (right) for Mach 14 air flow over viscous-optimized waverider at 100 km altitude with Kn = 0.02.

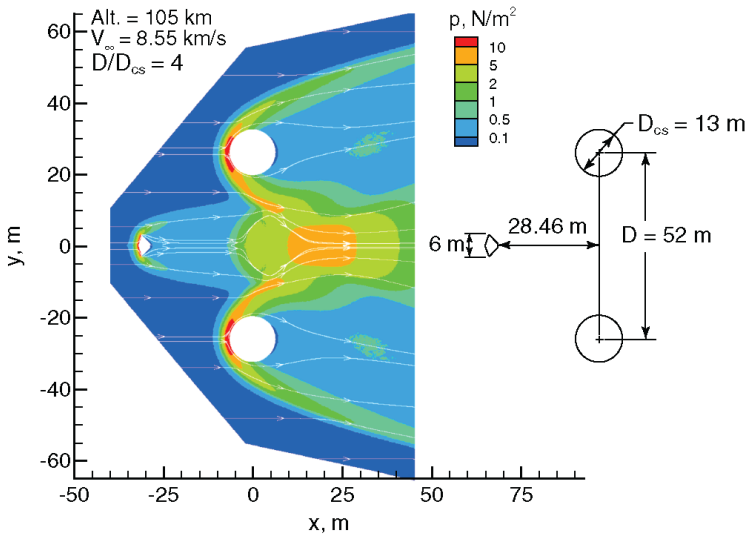

Figure 18: Pressure contours and streamlines for ballute atmospheric entry configuration [87].

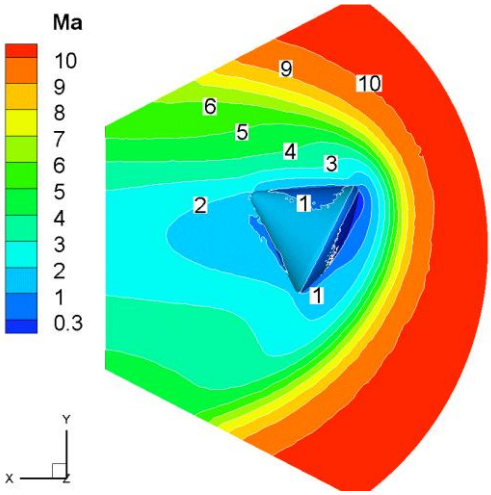

Figure 19: Contours of Mach number for Mach 10 flow of N_2 over Apollo command module geometry at 30° angle of attack, with Kn = 0.067 [88].

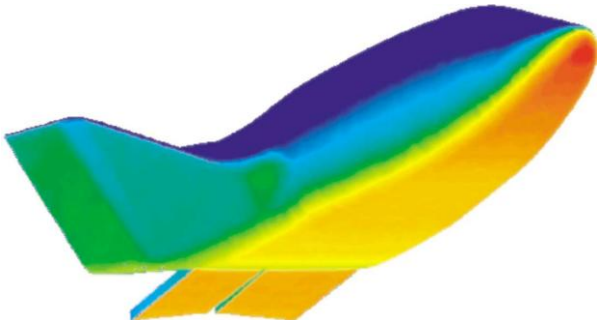

Figure 20: Surface pressure for X-38 reentry vehicle at 400,000 ft altitude [40].

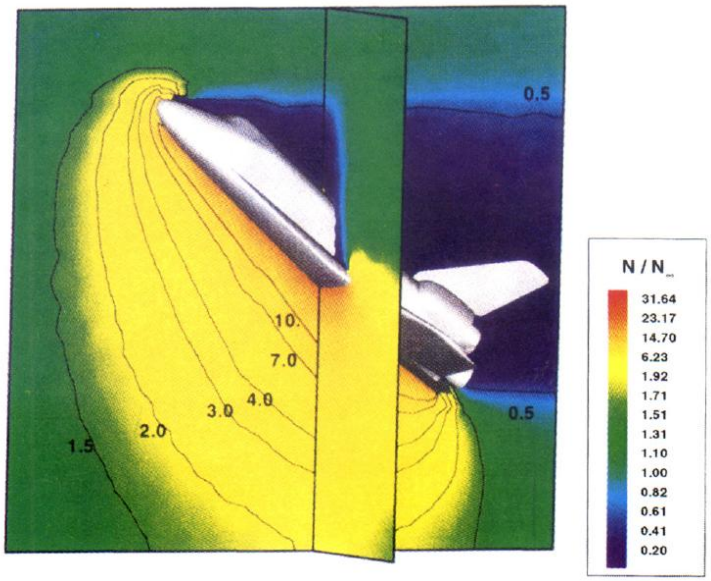

Figure 21: Density contours for Space Shuttle Orbiter at 170 km altitude [89].

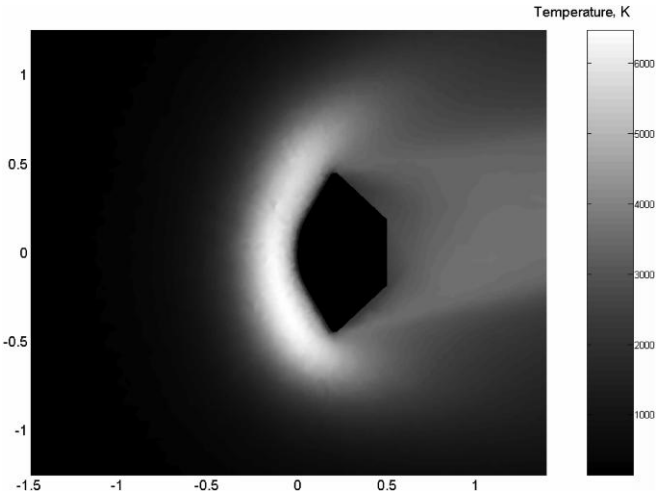

Figure 22: Overall temperature contours for Beagle2 entry into Mars atmosphere, with 11° angle of attack and Kn = 0.0291 [90].

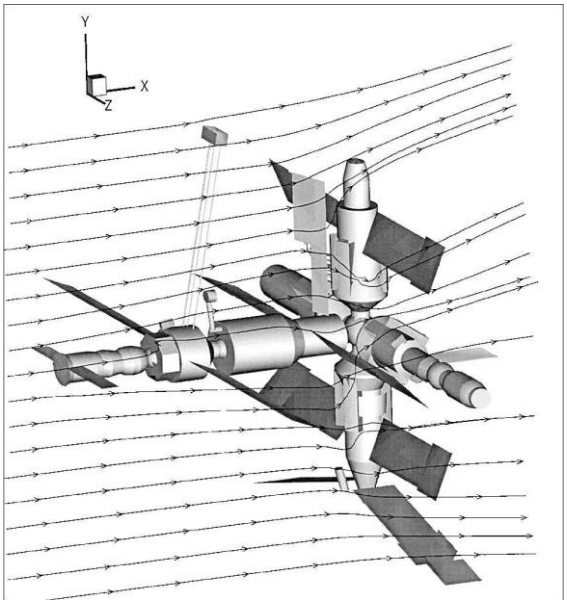

Figure 23: Streamlines from DSMC calculation of flow around Mir space station during controlled descent, at 110 km altitude [91].

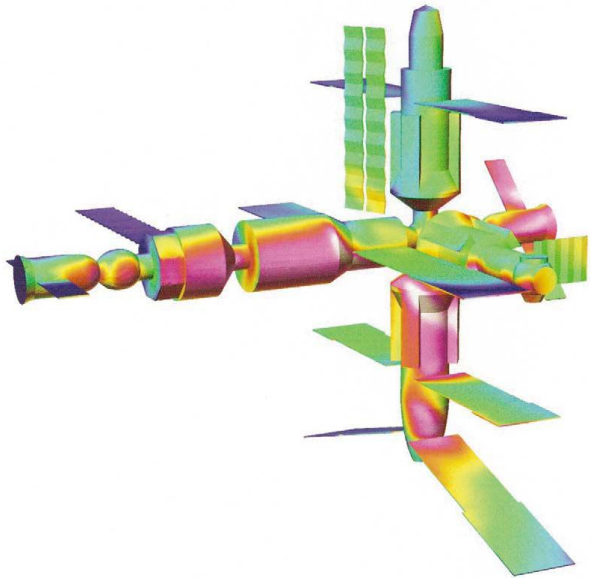

Figure 24: Surface pressure on Mir space station from Space Shuttle RCS exhaust during docking maneuver [40].

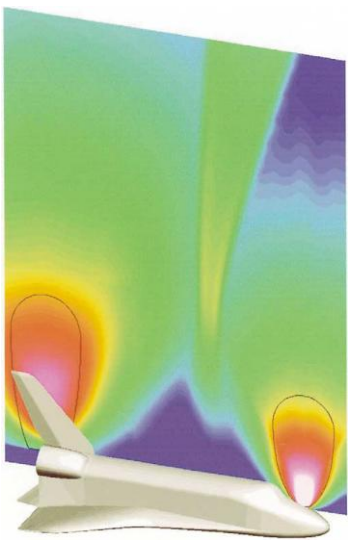

Figure 25: Centerline density distribution for uncoupled DSMC/CFD simulations of Space Shuttle Orbiter during simultaneous firing of RCS thruster in nose and two RCS thrusters in tail [40]. Black lines indicate DSMC/CFD domain boundaries.

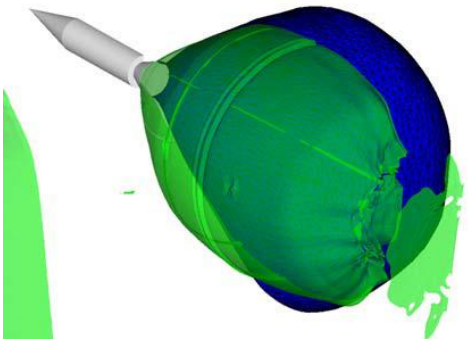

Figure 26: Continuum breakdown surface (green) and DSMC inflow boundary (blue) used for two-step CFD/DSMC simulation of rocket exhaust plume at high altitude [92].

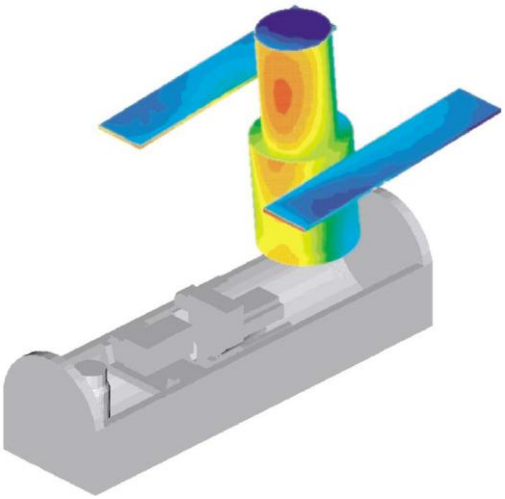

Figure 27: Pressure distribution over Hubble Space Telescope due to venting from Space Shuttle airlock during servicing mission [40].

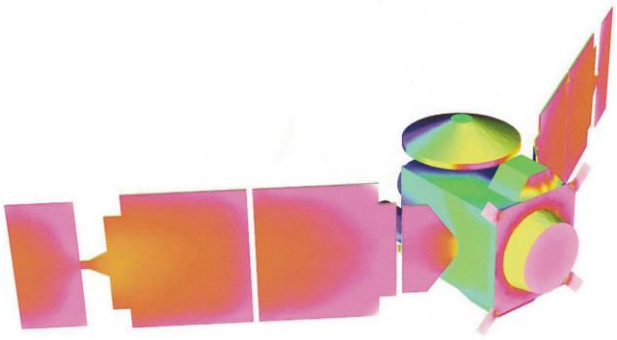

Figure 28: Surface heat flux over Mars Global Surveyor during aerobraking in Mars upper atmosphere [40].